Thermo-mechanical delamination analysis by a plate model with “adaptive” representation of displacements and temperature

THERMO-MECHANICAL DELAMINATION ANALYSIS BY A PLATE MODEL WITH "ADAPTIVE" REPRESENTATION OF DISPLACEMENTS AND TEMPERATURE

Ugo ICARDI

Dipartimento di Ingegneria Meccanica e Aerospaziale-DIMEAS
Politecnico di Torino – Corso Duca degli Abruzzi 24, 10129 Torino, Italy
Tel : +39 011 0906872; fax: +39 011 0906899

E-mail addresses: ugo.icardi@polito.it

Abstract

Progressive delamination failure under thermo-mechanical loading can led either to a premature failure or a consistent loss of strength and stiffness of laminated and sandwich composites in service. Customary, three-dimensional finite element models are used to predict the stress fields with the highest accuracy, while the behavior of the delamination crack is simulated by fracture mechanics or cohesive interface models. Because impact loading requires the solution of thousand iterations under the contact time, these models may overwhelm the computational capacity. The last generation of refined plate models which accurately capture the stress fields with a lower computational effort should be used for investigating impacts. Here a recently developed multilayered zig-zag thermo-elastic model is applied to the analysis of delamination problems under impact and thermal loading. The characteristic feature of this thermo-structural model, which *a priori* fulfills the equilibrium of out-of-plane stresses at the interfaces and the heat conduction equation, is the hierarchic representation of displacements and temperature across the thickness, though the number of functional d.o.f. is fixed in order to limit the memory storage occupation. As customary, the onset of delamination is computed using stress based criteria, but instead of simulating the delamination growth degrading the elastic properties of the failed regions, i.e. guessing suited multiplication factors, a mesoscale model is used which accurately and efficiently accounts for the damage. The strain energy updating technique by the author is used to develop an efficient C° finite element model. Results show good accuracy and low cost of the present approach.

INTRODUCTION

Laminated and sandwich composites are increasingly finding use in many engineering applications, owing to their excellent thermo-mechanical properties, low weight and the possibility to meet a wide range of design requirements by properly choosing the fiber orientation and the stacking lay-up.

As these materials exhibit elastic moduli and strengths in the thickness direction that are much smaller compared to those in the in-plane direction, warping, shearing and straining deformations of the normal and out-of-plane stresses rise, which should be accurately described by the models used for the simulations. A comprehensive discussion of the mechanisms of damage formation and evolution and of their modelling is given in the papers by Foo et al. [1], Tita de Carvalho and Vandepitte [2], Tay et al. [3], Garnich and Akula Venkata [4], Liu and Zheng [5] and Faggiani and Falzon [6]. Delamination, that is the failure of the resin film bonding adjacent plies or faces to core which largely influence stiffness, failure behaviour, service life and structural collapse, has been investigated by many authors, in order to accurately predict the response and to re-evaluate the life of use of damaged composites. As examples the papers by Bolotin [7], Camanho and Matthews [8], Choi et al. [9], Lee et al. [10], de Borst and Remmers [11], Flesher and Herakovich [12], Davies et al. [13], Elder et al. [14], Wang and Karihaloo [15], Bulsara et al. [16] and the book by Daniel and Ishai [17] are cited. The comprehensive review of delamination models by Berthelot [18] shows that often delamination is studied using fracture mechanics models where the strain energy release rates are efficiently evaluated by modified versions of the crack closure integral. As alternative models, the cohesive zone models based on a traction-separation law (see, e.g., La Saponara et al. [19], Borg et al. [20], Nishikawa et al. [21], and Wang et al. [22]) and the continuum damage mesomechanics (see Ladevèze et al. [23], [24]) may be used. The structural response is usually simulated by three-dimensional finite element discretizations, as delamination involves three-dimensional, locally evolving stress states. The papers by Chakraborty [25], Roy and Chakraborty [26] and Panigrahi and Pradhan [27] are cited as examples. Refined plate models with a lower computational effort and their counterpart elements are also successfully employed (see, e.g., Palazotto et al. [28], Kärger et al. [29], Diaz Diaz et al. [30] and Icardi and Ferrero [31]). An extensive assessment of these models and of their finite element counterparts is given in the papers by Noor and Malik [32], Zhang and Yang [33], Reddy and Arciniega [34] and Ghugal and Shimpi [35] and in the book by Reddy

[36]. It is just reminded that the plate models may have a number of d.o.f. depending on the number of layers, or have a fixed number of d.o.f. In the former case, the representation can be refined across the thickness, thus accuracy is generally better, but the computational effort is larger. In the latter case, good accuracy and low computational costs are obtained through algebraic transformations and a suited choice of the functional d.o.f., as discussed in the next section.

Thermal stresses which rise owing to anisotropic thermal expansion coefficients that vary from ply to ply, from faces to core and from fibers to matrix in a ply are a major concern in the engineering applications, since they may retard or enhance the onset and growth of delamination, or even be sufficiently large to cause failure, as extensively discussed in the recent books by Noda et al. [37] and Hetnarski and Eslami [38]. The following studies dealing with thermo-elastic effects of composites have been recently published. Hashemi et al. [39] have carried out parametric studies of the effects of temperature on individual and mixed-mode interlaminar fracture, fiber bridging, micro-cracking and plastic deformation, Fiedler et al. [40] have investigated the influence of thermal stresses on the transverse strength, while Sayman [41] studied the hygrothermal effcts in thick multilayered composites, Nairn [42] investigated the effects of thermal stresses on the interlaminar fracture behavior, Aghdam and Khojeh [43] considered the curing stresses in the analysis of the yielding behavior and Shu [44] investigated the thermo-elastic response of a laminate with imperfectly bonded layers.

The most recently published thermo-elastic delamination studies are based on fracture mechanics models and 3-D finite elements as structural models. Thermo-mechanically loaded composites with an elliptical embedded delamination observed from experiments were considered by Panda and Pradhan [45, 46], while an annular shaped delamination around a circular hole, which is due to drilling, was studied by and Babu and Pradhan [47]. A coupled thermo-mechanical finite element analysis of composite laminates with bridged delamination cracks loaded by a temperature gradient was carried out by Hattiangadi and Siegmund [48] using a cohesive zone model. At the author's best knowledge, no thermo-elastic delamination studies have been published where continuum damage mesomechanic models are used as damage models, as well as no application of the last generation of refined zig-zag plate models as thermo-structural models can be found. Hence, studies are required to understand whether these damage and structural models with a low computational effort may be convenient for

investigating delamination under impact loading, in presence of temperature gradients across the thickness.

To contribute to fill this gap, in this paper the 3-D zig-zag plate model with "adaptive" representation of displacements and temperature recently developed by the author [49] is used as thermo-structural model, while the damage mesoscale model by Ladevezè et al. [24] is employed as damage model. As customary for impact studies, the onset of delamination is computed using stress based criteria, being the only ones admissible for running within the innumerable time steps required for the analysis. The Choi-Chang's criterion is chosen as delamination criterion because a plenty of applications have shown it to provide accurate results, while the homogenization process by the damage mesoscale model is used to account for the stress concentration due to the delamination crack. Thus, instead of simulating the delamination growth by degrading the elastic properties of the failed regions according to the ply-discount theory [28-31], the residual properties are computed at any time strep by the damage mesoscale model. In this way, it is not required to guess parameters like the exponents that degrade the elastic properties of the failed regions in the ply-discount theory. In order to treat lay-ups, loading and boundary conditions of general interest, the thermo-structural model is implemented within the framework of the strain energy updating technique (SEUPT) recently developed by the author [50]. The reasons for the present choices are discussed into details hereafter.

(i) The structural model uses just the mid-plane displacements and shear rotations and the temperatures at the upper and lower bounding faces as functional d.o.f. in order to limit the memory storage occupation, nevertheless it *a priori* fulfils the heat conduction equation and the continuity of transverse shear and normal stresses at the interfaces, as prescribed by the elasticity theory for keeping equilibrium, and the adaptive terms enable a refinement across the thickness. Therefore, this model is chosen because it has the minimal number of functional d.o.f. though it accurately and quickly predicts the interlaminar stress fields.

(ii) SEUPT, which consists of a post-processing technique that locally improves the results by a preliminary finite element analysis carried out with standard shear deformable plate elements, gives rise to an efficient C° finite element model because no unwise derivatives of primary variables are required as nodal d.o.f., on the contrary of the direct implementation of the zig-zag model into the finite element scheme. The computational cost are saved because the updating

operations are just carried out locally and are fast. Besides, the standard nodal d.o.f. being used, the memory storage occupation is minimal.

(iii) Owing to the use of the damage mesoscale model, the effects of formation and growth of delamination cracks can be taken into account like with fracture mechanics and cohesive zone models, though the progressive failure analysis is still carried out with stress-based criteria, as customary. Another advantage is that using the damage mesoscale model, the residual properties are computed, instead of being guessed through an appropriate choice of the exponents that degrade the elastic properties, like with the ply-discount theory. The discretely damaged medium is replaced with a continuous homogeneous medium that is equivalent from an energy standpoint. The progressive failure analysis is carried out by using the stresses that results by the incorporation into the expression of the strain energy of damage indicators computed as the homogenized result of damage micromodels.

This paper is structured as follows. In order to put it in the right perspective, first the basic features of the available models used for simulating the thermo-elastic response of laminated and sandwich composites are briefly reviewed. Next, assumptions and basic features of the present termo-structural model are discussed along with those of the damage mesoscale model [24] used for simulating the progressive failure behavior. Afterwards, impact problems taken from the literature and the thermo-elastic delamination problem by Hattiangadi and Siegmund [48] are solved with the purpose to assess correct implementation and accuracy of the actual model. Finally, the former impact problems are reconsidered under temperature fields.

REQUIREMENTS

As mentioned in the introductory section, warping, shearing and straining deformations of the normal, which constitutes the so-called zig-zag effects, rise in laminated and sandwich composites because their elastic moduli and strengths in the thickness direction are much smaller compared to those in the in-plane direction. Since the zig-zag effects may largely influence the local and the overall behaviour, they should be accurately accounted for in the simulations. The displacement are required to be continuous at the

layer interfaces and to have appropriate discontinuous derivatives for satisfying the equilibrium equations, while the temperature and the heat flow should be continuous in order to satisfy the heat conduction equations. Many models have been developed that fully or partially satisfy these requirements. As many comprehensive review papers that address the modeling of thermo-structural problems are available, here only the basic features of the main classes of models are summarized, focusing the discussion on their number of functional d.o.f., accuracy and computational costs.

In the past, just linear or polynomial displacement and temperature fields were postulated across the thickness, assuming the displacements and the shear rotations at the mid-plane as functional d.o.f. and the temperature at the upper and lower bounding faces and, in many cases, at intermediate points across the thickness as thermal functional d.o.f. As the polynomials used to represent the variation of the d.o.f. across the thickness have continuous derivatives, the interlaminar stresses cannot be continuous, as prescribed by the elasticity theory, so equilibrium is not satisfied at the interfaces. Nevertheless, these simple and numerically efficient models may give accurate stress predictions, since the out-of-plane stresses can be computed integrating the local differential equilibrium equations starting from the in-plane stresses. Indeed, the in-plane stresses are generally accurately predicted because theya are not required to be continuous at the interfaces. However, cases exist for which post-processing could not provide accurate predictions [51], so the out-of-plane stresses should be computed by the constitutive equations. Models with a piecewise representation of displacements and temperature have been recently developed to this purpose, which satisfy the equilibrium and the heat conduction equations either in a point form or in an integral form. Because the models whose discretisation is independent of the material properties can yield inaccurate results even for thin laminates, usually a representation that allows for a refinement across the thickness is adopted, thus the number of functional d.o.f., the computational effort and the accuracy depend on the representation adopted. In the case of discrete-layer models, each layer is described separately as a plate and the contact conditions are enforced at the interfaces as constraint conditions. Refinement is obtained increasing the number of computational layers used to describe each physical layer. Mixed and hybrid models of this type that feature separate piecewise variations of displacements and stresses are as widespread as displacement based models, but also three-dimensional finite element models are largely used. Overloading computations may be incurred with these models because a large number of thin constituent plies are used to made laminates, which should

be discretized separately. A concern with 3-D FEA is keeping a reasonable aspect ratio of solid elements because, as mentioned, the constituent plies are generally thin and in many cases the resin film bonding adjacent plies should be discretized. The problem may be overcome by using interface elements or the boundary element method, as no thickness-order limitations are involved. However, 3-D FEA provides the most accurate results with arbitrary geometries, lay-ups, loading and boundary conditions, no assumptions being introduced that could limit accuracy.

The discrete-layer models can be as accurate as exact 3-D solutions and 3-D FEA, but also similarly expensive as they give a separate representation of displacements and temperature across any computational/physical layer. Models that offer a 3-D description by a discrete-layer model just in the regions of interest and a partial modelling capability outside, like the hierarchical and the predictor-corrector models, are used to limit the computational effort [32].

Refined plate and shell models that may be used in place of 3-D FEA and discrete-layer models have been recently developed for solving thermo-elastic problems. They are here referred as the zig-zag models, Their displacement fields have appropriate discontinuous derivatives in order to make the interlaminar stresses continuous at the interfaces, for keeping equilibrium. Generally, a high-order piecewise variation of the in-plane displacements is assumed across the thickness with the purpose of accounting for the effects of transverse shears, while the transverse displacement is usually assumed constant, linear or parabolic since the major concern is to contain memory storage occupation and processing time. Their characteristic feature is an *a priori* fulfilment of the stress contact conditions at the interfaces by the incorporation of continuity functions into the displacement fields whose expressions are computed once for all for any lay-up. These models, which have a fixed number of functional d.o.f., have been initially developed to account just for the continuity of transverse shear stresses [52], since it has important effects on the overall response. They have been refined incorporating either a global-local superposition of displacement fields [53], to obtain accurate stress predictions from the constitutive equations, or a sublaminate representation [54] which can be refined across the thickness, though at the expense of an increased n umber of functional d.o.f.

It could be noticed that the transverse displacement should be variable across the thickness, since the transverse normal stress has a significant bearing for keeping equilibrium in thermo-elastic problems. Because also the temperature should have appropriate

discontinuous derivatives at the layer interfaces in order to satisfy the continuity of the heat flux at the interfaces of materials with different thermo-elastic properties and the heat flux equation, zig-zag models of the temperature have been recently developed by Kapuria et al. [56] and Oh and Cho [57]. In [56], a beam model with a piecewise cubic representation of the in-plane displacement is used that *a priori* satisfy the continuity of the transverse shear, while the transverse displacement is approximated by integrating the constitutive equation for the transverse normal stress. The temperature profile is described solving the heat conduction equation with a sub-layerwise approximation in terms of the temperatures at the upper and lower bounding faces and of temperatures at intermediate points across the thickness. The transverse displacement is constructed including only the thermal contribution, since this contribution to the transverse normal strain is much greater than the one by the transverse normal stress for moderately thick laminates. In [57], a finite plate element for analysis of thermo-piezo-elastic problems is developed in which the temperature and the in-plane displacements are approximated by zig-zag cubic variations across the thickness, while the transverse displacements is assumed as a cubic polynomial, thus the transverse normal stress is discontinuous at the interfaces. The temperature variation is described assuming the temperature at the upper and lower bounding faces and by enforcing the heat flux boundary conditions on top and bottom surfaces and the continuity of the heat flux at each interface.

The author [49] has recently developed a 3-D thermo-elastic zig-zag model which *a priori* fulfils the continuity of transverse shear and normal stresses and of the transverse normal stress gradient at the interfaces, the heat conduction equation and the continuity of the temperature, as required for keeping equilibrium and fulfilling the heat conduction equation. Its characteristic feature is that it can be refined across the thickness keeping unchanged the number of functional d.o.f., in order to limit the memory storage occupation. Though the representation of displacements and temperature can be different from point to point across the thickness, with the aim to adapt to the variation of solutions, the number of functional d.o.f. is kept fixed because the coefficients of displacements and temperature are expressions of the functional d.o.f. obtained by enforcing the equilibrium conditions and the fulfilment of the heat conduction equation at intermediate points across the thickness. This avoids an increased number of primary variables when the representation is refined across the thickness, so no increase of the memory storage dimension occurs. In order to make the model efficient, the algebraic operations required for determining the expressions of these coefficients are actually carried out once at a time in analytic form using a symbolic calculus tool. To have the minimal number

of variables, the mid-plane displacements, the shear rotations and the temperatures at the upper and lower faces are chosen as functional d.o.f..

Applications have shown that though the the model requires the computation of continuity functions and coefficients of adaptive terms, its overall processing time is shorter of that of counterpart models where the zig-zag contributions and the adaptive terms are omitted, because long post-processing operations are required by these simplified models to achieve the same accuracy [58].

Comparison with exact thermo-elasticity solutions demonstrated that very accurate predictions can be obtained from constitutive equations, even for laminates with a length-to-thickness ratio of two and distinctly different properties of layers, as well as for sandwiches [49]. The memory storage dimension is nearly equal to that of simplified models with the same d.o.f., but accurate results are obtained in a shorter time. Because the adaptive model have a smaller number of functional d.o.f. than discrete-layer and sublaminate ZZ models, but achieves a comparable accuracy from constitutive equations, it represents a good alternative opportunity toward a reduction of the overall computational effort.

Here an application is presented to thermo-elastic delamination problems. As a necessary premise, the basic features of displacement and temperature models are summarized, then the strain energy updating technique is used for developing the finite element model employed in the applications, afterwards the damage model is discussed, finally the numerical results are presented.

THERMO-STRUCTURAL MODEL

As a detailed discussion of the thermo-structural model is given in [49], only the basic relations, assumptions and motivations are reminded hereafter.

Structure

Consider a laminated or sandwich plate of sides L_α, L_β and thickness H. The following piecewise representation of the displacements is assumed across the thickness:

$$u_\alpha(\alpha,\beta,\zeta)=u_\alpha^{(0)}(\alpha,\beta)-\zeta u_{\zeta,\alpha}^{(0)}(\alpha,\beta)+\zeta\left(1+\left(C_{2\alpha}(\alpha,\beta)\zeta+C_{3\alpha}(\alpha,\beta)\zeta^2\right)\right)\gamma_\alpha^{(0)}(\alpha,\beta)+$$
$$(\mathrm{O}\,\zeta^4.....)+\sum_{k=1}^{S}\Phi_\alpha^{(k)}(\alpha,\beta)\left(\zeta-\zeta^{(k)}\right)\mathrm{H}_{.k}\left(\zeta-\zeta^{(k)}\right) \qquad (1)$$

$$u_\beta(\alpha,\beta,\zeta)=u_\beta^{(0)}(\alpha,\beta)-\zeta u_{\zeta,\beta}^{(0)}(\alpha,\beta)+\zeta\left(1+\left(C_{2\beta}(\alpha,\beta)\zeta+C_{3\beta}(\alpha,\beta)\zeta^2\right)\right)\gamma_\beta^{(0)}(\alpha,\beta)+$$
$$(\mathrm{O}\,\zeta^4.....)+\sum_{k=1}^{S}\Phi_\beta^{(k)}(\alpha,\beta)\left(\zeta-\zeta^{(k)}\right)\mathrm{H}_{.k}\left(\zeta-\zeta^{(k)}\right) \qquad (2)$$

$$u_\zeta(\alpha,\beta,\zeta)=a(\alpha,\beta)+\zeta b(\alpha,\beta)+\zeta^2 c(\alpha,\beta)+\zeta^3 d(\alpha,\beta)+\zeta^4 e(\alpha,\beta)+\quad(\mathrm{O}\,\zeta^5.....)+$$
$$\sum_{k=1}^{S-1}\Psi_\zeta^{(k)}(\alpha,\beta)\left(\zeta-^{(k)}\zeta\right)\mathrm{H}_k\left(\zeta-\zeta^{(k)}\right)+\sum_{k=1}^{S-1}\Omega_\zeta^{(k)}(\alpha,\beta)\left(\zeta-^{(k)}\zeta\right)^2\mathrm{H}_k\left(\zeta-\zeta^{(k)}\right) \qquad (3)$$

where the meaning of symbols is as follows. The in-plane coordinates α,β over the reference middle surface Ω and the coordinate ζ across the thickness are assumed as reference system. The elastic displacement components in the direction of α,β and ζ are indicated with the symbols u_α, u_β, u_ζ, respectively. The three displacements $u_\alpha^{(0)}$, $u_\beta^{(0)}$, $u_\zeta^{(0)}$ and the two shear rotations $\gamma_\alpha^{(0)}$, $\gamma_\beta^{(0)}$ of the points on the reference surface Ω are chosen as functional d.o.f. H_k is the Heaviside unit step function ($\mathrm{H}_k\left(\zeta-\zeta^{(k)}\right)$ =1 for $\zeta \geq \zeta^{(k)}$ and 0 for $\zeta < \zeta^{(k)}$) which makes piecewise continuous the displacements, and $\zeta^{(k)}$ are the coordinates of the interfaces. $C_{2\alpha}, C_{3\alpha}, C_{2\beta}, C_{3\beta}$ are coefficient whose expressions are obtained by enforcing the transverse shear stress-free boundary conditions at the upper and lower free surfaces, *a* plays as the transverse displacement $u_\zeta^{(0)}$ on the reference mid-plane, coefficients *b* to *e* are determined by enforcing the boundary conditions on the transverse normal stress and stress gradient at the upper and lower bounding surfaces.

With an appropriate definition of the continuity functions $\Phi_\alpha^{(k)}$, $\Phi_\beta^{(k)}$, $\Psi_\zeta^{(k)}$, $\Omega_\zeta^{(k)}$ the displacement fields defined above *a priori* fulfill the continuity of the transverse shear and normal stresses at the interfaces and the continuity of the transverse normal stress gradient across the thickness, as required by the elasticity theory for satisfying the equilibrium conditions. The expressions of the continuity functions are determined in a

straightforward way (once for all for any lay-up) in terms of the functional d.o.f. and the elastic properties by enforcing the continuity of transverse shear and transverse normal stresses and of the transverse normal and stress gradient $\sigma_{\zeta\zeta,\zeta}$ at the interfaces. The latter condition follows in a straightforward way from the local differential equilibrium equations, but it is usually disregarded in order to limit the computational effort, despite it gives not negligible contributions when the material properties vary in ζ. Notice that a piecewise variation is here assumed also for the transverse displacement since it is fundamental when thermal stresses rise, as discussed above. The differentiations with respect to the spatial coordinates have been denoted by $(\ )_{,\alpha}$, $(\ )_{,\beta}$, $(\ )_{,\alpha\zeta}$ in the previous relations,.

The high-order terms $(O\zeta^4.....)$, $(O\zeta^5.....)$ represent "*adaptive*" contributions to the displacements

$$P^m{}_J(H_{m-1} - H_m) + \ldots + P^n{}_J(H_{n-1} - H_n) + \ldots \qquad (4)$$

$P^n{}_J$ and $P^m{}_J$ being polynomials defined apart for any displacement component ($J \equiv \alpha$, β, ζ), whose order *m, n* can be different from point-to point across the thickness

$$P_\alpha{}^\upsilon = A^\alpha\zeta^4 + B^\alpha\zeta^5 + C^\alpha\zeta^6 + D^\alpha\zeta^7 + E^\alpha\zeta^8 + \ldots \qquad (5)$$

$$P_\beta{}^\nu = A^\beta\zeta^4 + B^\beta\zeta^5 + C^\beta\zeta^6 + D^\beta\zeta^7 + E^\beta\zeta^8 + \ldots \qquad (6)$$

$$P_\zeta{}^\nu = A^\zeta\zeta^5 + B^\zeta\zeta^6 + C^\zeta\zeta^7 + D^\zeta\zeta^8 + E^\zeta\zeta^9 + \ldots \qquad (7)$$

It is supposed that a polynomial of order *m* is employed for a group of layers, while a polynomial of order *n* is used for the adjacent layers, but the same representation can also be used across the thickness. The in-plane displacements are expressed by polynomials $P_\alpha{}^\upsilon$, $P_\beta{}^\nu$ of the same order (the symbol ν is used for representing in turns *m* and *n*), while a different representation $P_\zeta{}^\nu$ is used for the transverse displacement. The coefficients $A^\alpha \ldots E^\alpha$, $A^\beta \ldots E^\beta$, $A^\zeta \ldots E^\zeta$ are determined by enforcing equilibrium conditions at a desired number of intermediate points across the thickness. Since the displacement and stress fields can adapt to the variation of solutions across the thickness, the interlaminar stresses can be always accurately predicted from constitutive equations, thus post-processing operations are unnecessary.

With an appropriate choice of "*adaptive*" contributions, Poisson's locking approaching the thick limit and shear locking approaching the thin limit may be prevented, as well as the poor behavior of models with displacements and shear rotations as functional d.o.f., since a non-vanishing transverse shear can be enforced though the displacement d.o.f. and their derivatives vanish.

Temperature

The temperature $T(\alpha,\beta,\zeta)$ should be continuous and have appropriate discontinuous gradients in ζ at the layer interfaces, because the heat flux should be continuous. According, the temperature variation is approximated as the product of an in-plane function $\tilde{C}(\alpha,\beta)$ and a function $\overset{*}{T}(\zeta)$ across the thickness

$$T(\alpha,\beta,\zeta) = \tilde{C}(\alpha,\beta)\ \overset{*}{T}(\zeta) = \tilde{C}(\alpha,\beta)\ [\tilde{\Im}(\zeta) + \sum_{k=1}^{s}\Delta^{(k)}(\alpha,\beta)(\zeta-\zeta^{(k)})\mathsf{H}_{k}\left(\zeta-\zeta^{(k)}\right)] \quad (8)$$

with the following properties [49]. $\tilde{C}(\alpha,\beta)$ is a continuous function with continuous gradients in (α, β), since the thermo-elastic properties of laminated and sandwich composites have a smooth in-plane variation. The piecewise function $\overset{*}{T}(\zeta) = \tilde{\Im}(\zeta) + \Im'(\zeta)$ is constructed summing a contribution $\tilde{\Im}(\zeta)$ that is continuous and has a continuous gradient in ζ to a zig-zag contribution with discontinuous gradients at the layer interfaces, $\Im'(\zeta) = \sum_{k=1}^{s}\Delta^{(k)}(\alpha,\beta)\ (\zeta-\zeta^{(k)})\mathsf{H}_{k}\left(\zeta-\zeta^{(k)}\right)$. The contribution $\tilde{\Im}(\zeta)$ is expressed as the superposition of a linear variation in ζ between the temperatures at the upper and lower bounding faces T^{U} and T_{L}, respectively, which constitute the thermal d.o.f. to a polynomial representation with a variable order in ζ that represents the "*adaptive*" part of the temperature model

$$\tilde{\Im}(\zeta) = \frac{\zeta}{h}T_{L} + (1-\frac{\zeta}{h})T^{U} + ({}_{2}A^{T}\,{}_{2}N + \ldots. + {}_{n}A^{T}\,{}_{n}N + {}_{m}A^{T}\,{}_{m}N) \quad (9)$$

Each "*adaptive*" term is represented as a polynomial expansion:

$$ {}_m A^T \, {}_m N = \overset{1}{\Theta}^2 \zeta^2 + \overset{1}{\Theta}^3 \zeta^3 + ... + \overset{1}{\Theta}^n \zeta^n + \overset{1}{\Theta}^m \zeta^m \qquad (10) $$

whose coefficients $\overset{1}{\Theta}^2, \ldots, \overset{1}{\Theta}^m$ are determined as functions of the thermal d.o.f. T^U and T_L by enforcing the fulfilment of the heat conduction equation at intermediate points across the thickness.

The appropriate expressions of the thermal continuity functions $\Delta^{(k)}$ are determined in a straightforward way by enforcing the heat flux continuity at the interfaces. The heat flux continuity conditions can be written in a recursive form that is easily tractable and allows to determine $\Delta^{(1)}$, $\Delta^{(2)}, \ldots, \Delta^{(k)}$ in sequence, starting with the computation of $\Delta^{(1)}$ as the only unknown at the first interface, then with $\Delta^{(2)}$ as the only unknown at the second interface and so on.

The thermal continuity functions $\Delta^{(k)}$ and the unknown coefficients $\overset{1}{\Theta}^2, \ldots, \overset{1}{\Theta}^m$ are simultaneously determined by solving the algebraic system that results from the enforcement of the continuity of the heat flux at the layer interfaces and the Laplace's equation at points arbitrarily located across the thickness, whose number should be chosen equal to the number of unknown coefficients. This system consists of a set of relations that involve the temperature d.o.f. T^U, T_L, the thermal properties and derivatives of $\tilde{C}(\alpha, \beta)$ and $\tilde{\mathfrak{I}}(\zeta)$.

In order to make the model efficient , the continuity functions appearing in the displacement and temperature fields and the coefficients of the adaptive contributions are determined using a symbolic calculus tool, since an "analytic" expression is determined once for all which saves time because it is just substituted instead of being computed in any application.

It could be noticed that, the interlaminar stress and the heat flux continuity conditions should be enforced also at all the points where the representation is varied across the thickness, because the properties do not vary but the expressions of displacements and temperature have been changed.

The possibility of choosing a different order of representation from point to point across the thickness enables the treatment of multilayered materials with distinctly different thermal properties using just two temperature d.o.f. , so the refinement is still made without any increase of the number of primary variables, like for displacements. As no post-processing operations, stacking of computational layers, or computation of

additional thermal and displacement primary variables are required, temperature profile, stresses and displacements are efficiently computed.

Strain energy updating

For treating lay-ups, loading and boundary conditions of general interest, a finite element model should be developed. Unfortunately, a direct implementation of the present structural model involves derivatives of the displacements as nodal d.o.f. To overcome this problem, the strain energy updating technique (SEUPT) by the author [31], [50] is applied. With this technique, which can be easily implemented within standard finite elements computer codes, the results of a preliminary finite element analysis by standard shear deformable plate elements, here referred as the parent finite element analysis (PFA), are improved using the present thermo-structural model. In a broad outline, the results of PFA are interpolated in the regions of interest using spline functions, then this interpolation is used to construct an updated "analytical" solution, as outlined hereafter. An advantage of SEUPT is that laminates with distinctly different properties of constituent layers, strong anisotropy significant transverse normal stresses and strains and loading and boundary conditions of general interest can be treated using commercial finite element codes, as their accuracy is updated up to the level of the zig-zag model. Using SEUPT, no derivatives of displacements are involved as nodal d.o.f. because differentiation, integration and any other operation necessary for constructing the solution are carried out on the spline interpolation instead of being carried out on the finite element interpolation functions. According, computationally efficient C° shear deformable elements with the customary displacements and shear rotations as nodal d.o.f. and efficient linear or parabolic functions standard interpolating functions can be employed in the PFA phase. Of course, reduced integration, or better, the inconsistent spurious constraints should be removed from these elements for avoiding shear locking. The present structural model does not suffer from locking because the transverse displacement, its derivatives and the transverse shear rotations are not interpolated separately.

In the version of SEUPT used in this paper, three sets of updating operations are separately carried out over the strain energy, the work of external forces and the kinetic energy. It could be noticed that because the actual structural model does not need integration of differential equilibrium equations for predicting the interlaminar stresses,

the updating procedure is faster than in [31], [50] and no derivatives of the in-plane stresses are involved.
The expressions of strain and kinetic energies and of the work of external forces are constructed using a symbolic calculus tool, since the energy balance is written in analytical form once at a time outside the solution process, making the computations faster. SEUPT consists of the following steps.

- First, the overall rotations $\vartheta_\alpha = \gamma_\alpha^{(0)} - \zeta\, u_{\zeta\,,\alpha}^{(0)}$, $\vartheta_\beta = \gamma_\beta^{(0)} - \zeta\, u_{\zeta\,,\beta}^{(0)}$ used as functional d.o.f. by the finite elements in the PFA phase are made consistent with the actual structural model. To this purpose, the contributions of $\gamma_\alpha^{(0)}$, $\gamma_\beta^{(0)}$, $u_{\zeta\,,\alpha}^{(0)}$, $u_{\zeta\,,\beta}^{(0)}$ are separated from the spline interpolation of ϑ_α, ϑ_β. Next, the spline interpolation of $\hat{u}_\alpha^{(0)}$, $\hat{u}_\beta^{(0)}, \hat{u}_\zeta^{(0)}, \hat{\gamma}_\alpha^{(0)}, \hat{\gamma}_\beta^{(0)}$ are introduced in the expression of the strain energy. The purpose is computing the corrective terms $\Delta_\alpha^u, \Delta_\beta^u, \Delta_\zeta^u, \Delta_\alpha^\gamma, \Delta_\beta^\gamma$ that make the solution $\hat{u}_\alpha^{(0)} + \Delta_\alpha^u$, $\hat{u}_\beta^{(0)} + \Delta_\beta^u$, $\hat{u}_\zeta^{(0)} + \Delta_\zeta^u, \hat{\gamma}_\alpha^{(0)} + \Delta_\alpha^\gamma$, $\hat{\gamma}_\beta^{(0)} + \Delta_\beta^\gamma$ consistent with the actual structural model, simply substituting the expressions of the updated displacement into the energy balance for the actual structural model. It could be noticed that ill-conditioning of the spline interpolation may be easily overcome by suitably choosing the set of interpolation points, as so many points are available as alternative choices because the results being known at all nodes and gauss points. As shown by numerical tests, accurate results are obtained using a 4x4 interpolation scheme around the area of interest, which results in a third-order approximation over each patch, as shown in the previous applications [31] and [50]. If too many interpolation points are retained, oscillations can rise at the bounds of the sub-regions considered.

- Then the energy balance is constructed in order to compute $\Delta_\alpha^u, \Delta_\beta^u, \Delta_\zeta^u, \Delta_\alpha^\gamma, \Delta_\beta^\gamma$. First just the correction Δ_α^γ is incorporated in the energy balance, assuming all the other corrections to vanish. The work of the external forces, which comprises the thermal contribution computed with the temperature profile described above, is updated in a similar way substituting the expressions of the updated displacement d.o.f. Also the kinetic energy by the actual model is preliminary updated in the same way. The dynamic updating of the FSDT model is obtained

considering the work of inertial forces and the fact that corrections must hold irrespective of the time evolution of the solution, which is assumed in harmonic form. Once the first approximate Δ^{γ}_{α} is computed from the energy balance, it is used for computing Δ^{γ}_{β} in a similar way assuming all the other corrections still vanishing. The solution to this and following steps is obtained using the Penalty Function Method. Next corrections $\Delta^{u}_{\alpha}, \Delta^{u}_{\beta}, \Delta^{u}_{\zeta}$ are obtained introducing each term one at a time and reiterating the entire process till convergence.

- The membrane displacements are expected not to vary so much. However, Δ^{γ}_{α}, Δ^{γ}_{β} computed by updating the transverse shear energy, as described above, are used for improving the membrane energy, with the purpose of computing $\Delta^{u}_{\alpha}, \Delta^{u}_{\beta}$, Δ^{u}_{ζ} from the energy balance. Again, each correction is assumed once at a time, starting with the computation of Δ^{u}_{α} and assuming the remaining ones to vanish. The approximate expression of Δ^{u}_{α} computed by the energy balance is used for computing an approximate expression of Δ^{u}_{β} and both expressions of $\Delta^{u}_{\alpha}, \Delta^{u}_{\beta}$ are used for computing Δ^{u}_{ζ}. Then the entire process is restarted and repeated till convergence after having computed the contribution by the normal stress and strain, which are disregarded by the FSDT model used in the PFA phase, as described hereafter.

- An approximate expression of the transverse normal stress $\hat{\sigma}_{\zeta\zeta}$ is obtained from the results of the PFA analysis. In details, the spline representation of the transverse shear stresses by the FSDT model are derived in α, β and integrated in ζ, then an approximate expression of the transverse normal stress $\hat{\sigma}_{\zeta\zeta}$ is obtained by integrating the third local differential equilibrium equation. Then, an approximate expression of the transverse normal strain $\hat{\varepsilon}_{\zeta\zeta}$ is computed using the 3D stress–strain relation. The contribution by the normal stress and strain $\hat{\sigma}_{\zeta\zeta}$, $\hat{\varepsilon}_{\zeta\zeta}$ computed in this way are substituted into the energy balance and used for computing the corrective displacements as described above. $\hat{\sigma}_{\zeta\zeta}$, $\hat{\varepsilon}_{\zeta\zeta}$ computed

at the end of each primary iteration which starts with the computation of Δ^{γ}_{α} and finishes with the computation of Δ^{u}_{ζ} are used as entry values for the next iteration.

- The updating operations described above are carried out first disregarding the adaptive contributions to displacements given by the hierarchic terms, then these initially omitted contributions are computed as outlined hereafter. To this purpose, a sub-process is started after the computation in sequence of Δ^{γ}_{α}, Δ^{γ}_{β}, $\Delta^{u}_{\alpha}, \Delta^{u}_{\beta}$, $\Delta^{u}_{\zeta}, \overset{1}{\sigma}_{\zeta\zeta}$, $\overset{1}{\varepsilon}_{\zeta\zeta}$ as described above, in order to compute the hierarchic coefficients A^{α}, A^{β}, A^{ζ}, B^{α}, B^{β}, B^{ζ}, ... E^{ζ} by enforcing the local equilibrium equations at selected points across the thickness choosing a suitable subdivision scheme. Subdivisions may be refined across the thickness in the regions where a higher-order representation is required, however numerical tests have shown that this refinement is unnecessary for undamaged laminates and sandwiches.

- The previous updating operations are repeated till convergence after incorporation of the hierarchic terms. The entire process which started with the computation of Δ^{γ}_{α}, Δ^{γ}_{β} is repeated using the last correction as the entry solution for the next iteration, and the magnitude of corrective displacements $\Delta^{u}_{\alpha}, \Delta^{u}_{\beta}$, $\Delta^{u}_{\zeta}, \Delta^{\gamma}_{\alpha}$, Δ^{γ}_{β} as a measure of errors.

The numerical applications have shown that in all the examined cases very few iterations are required in each sub-cycle as well as in the entire process [31], [50]. The results obtained using SEUPT have shown that accurate results can be obtained with a little increase of the computational processing time by 20 % with respect to the direct application of the model (using the Galerkin's method), obtaining accurate results from constitutive equations even in the cases where integration cannot be successful [51].

Damage model

The purpose of this section is to summarize the features of the damage model employed

in the numerical applications. Because impact induced delamination is considered in the reference sample cases considered, a brief description of the technique for simulating impacts is premised to the discussion of the damage model, in order to justify the choices made.

The contact force model and the damage model represent the extension of the ones in [31] to the actual thermo-elastic model. In the present study, the residual properties are computed at any time step by a damage mesoscale model [24] which accounts for the stress concentration due to the delamination crack and computes the residual elastic properties through an homogenization process. The progressive failure analysis is still carried out with stress-based criteria, but instead to guess the exponents that the play-discount theory uses for representing the residual properties, like in [31], here the effects of formation and growth of delamination cracks are explicitly taken into account. To this purpose, a three-dimensional finite element analysis is carried out outside the impact simulation process, which computes the damage indicators [24] that multiply the strain energy components in order to account for the stress concentrations due to delamination cracks. In this way, the progressive failure analysis is carried out by using the stresses that results from the energy balance, as customary, but the effects of evolving damages are accounted for replacing the discretely damaged medium with a continuous homogeneous medium that is equivalent from an energy standpoint. As a consequence, the damage mechanism can be accurately simulated using a refined plate element with the standard nodal d.o.f., as shown in the numerical applications, instead of using 3-D FEA. As the homogeneization process is carried apart once at a time, this approach results in computational cost saving.

Impact loading

Dynamic loading due to the impact of foreign objects is a serious design concern even when velocity and energy are low, because it is always responsible for a relevant degradation of the structural properties. Local damage occurs as a visible permanent indentation in laminated composites, while global damage mainly consists of invisible extensive internal delaminations. In sandwich composites it occurs as an invisible crushing of core at low energies, which is followed by complete tearing of the impacted face at high energies.

Here just low velocity/low energy impact cases are considered. Their simulation is a rather complex matter that requires to account for a complex combination of local failures, crack propagation and post-failure behavior in the transient dynamics analysis and the estimation of the damage requires the solution of non-conservative, non-linear problems. In this paper, the indentation depth and the contact area are computed assuming the distribution of the contact force to be Hertzian, as customary. The projectile is described as a rigid body, while the effective stiffness of the target structure is simulated by FEA, instead of assuming a simplified structural model, as usual. This does not result in unaffordable costs because the solution to all the sample cases is found by SEUPT running few minutes on a laptop computer.

At any load increment, the solution of the contact problem proceeds as follows. The contact force F and the vertical displacement are assumed to vanish at the first instant of the contact. After a small time increment Δt, the contact force is assumed to reach the value $F=\Delta F$ and no damage is though to occur. As a consequence, the impactor moves on at a distance that depends on the nonlinear effective plate stiffness. In this phase, the contact force is assumed to be distributed over the contact area according to the Hertzian law. The contact radius, which provides the applied pressure corresponding to the load, is computed at each load step by an iterative algorithm that forces the top surface of the target to conform the shape of the impactor in the least-squares sense [28], like in [31]. The contact area radius computed in this way is assumed as the estimated contact radius for the next increment. The load is then incremented and the process repeated till the impactor and the indentation radii are in agreement, then the failure analysis is performed, as described hereafter.

The Newmark implicit time integration scheme is used for solving the dynamic equations, because the alternative explicit time integration schemes need extremely small time steps to be stable. However to limit convergence and rounding errors, quite small time-steps should be considered. As the solution depends on the current configuration, the previous history and, in addition, deformation can be locally quite large, a modified version of the Newton-Raphson method is used for solving the problem. The problem is linearized over any load increment considering the tangent $[K(q)]_T$ and the secant $[K(q)]_S$ stiffness matrices. In a broad outline, increasing the load at the next iteration to $F_{(i)}$, the solution at the previous iteration $q^o_{(i-1)}$ is no longer in equilibrium, thus a residual force R_i exists which is computed using the secant stiffness matrix

$$\left[K\left(q^{0}{}_{(i-1)}\right)\right]_S q^{0}{}_{(i-1)} - F_{(i)} = R_{(i)} \neq 0 \qquad (11)$$

The nodal d.o.f. vector $q^{o}{}_{(i\text{-}1)}$ is updated to $q^{0}{}_{(i)} = q^{0}{}_{(i-1)} + \Delta q_{(i)}$ computing $\Delta q_{(i)}$ from

$$\left[K\left(q^{0}{}_{(i-1)}\right)\right]_T \Delta q_{(i)} = R_{(i)} \qquad (12)$$

in order to make the structure in equilibrium with $F_{(i)}$. Using this procedure the contact force and its distribution over the variable contact area are efficiently and realistically computed, instead of using a fixed surface as customary. Adaptive mesh refinement could be used for improving accuracy, since the contact radius changes while the load varies according to the time history, but this option is left to a future study.

Failure criteria and mesoscale damage model

Macromechanical, stress-based criteria with a separate description of the various failure mechanism are the only failure models to date available that have reasonable costs for structures of technical interest. They represent a good compromise, being sufficiently accurate and requiring a sufficiently low computational effort to run thousand times during the time steps required for the analysis of impacts. As shown by plenty of papers, the failure of fibres and matrix can be accurately predicted using the 3D Hashin's criterion with in situ strengths. Tensile failure of fibres occurs if

$$\left(\frac{\sigma_{11}}{X^{t}}\right)^{2} + \frac{1}{S_{12=13}{}^{2}}\left(\tau_{12}{}^{2} + \tau_{13}{}^{2}\right) = 1 \qquad (\sigma_{11} > 0) \qquad (13)$$

while compressive failure occurs if

$$\sigma_{11} = -X^{c} \qquad (\sigma_{11} < 0) \qquad (14)$$

Matrix failure under traction occurs if

$$\left(\frac{\sigma_{22} + \sigma_{33}}{Y^{t}}\right)^{2} + \frac{1}{S_{23}{}^{2}}(\tau_{23}{}^{2} - \sigma_{22}\sigma_{33}) + \left(\frac{\tau_{12}}{S_{12=13}}\right)^{2} + \left(\frac{\tau_{13}}{S_{12=13}}\right)^{2} = 1 \qquad (\sigma_{22} + \sigma_{33} > 0) \qquad (15)$$

while matrix failure under compression occurs if

$$\frac{1}{Y^c}\left[\left(\frac{Y^c}{2S_{23}}\right)^2-1\right](\sigma_{22}+\sigma_{33})+\frac{1}{4{S_{23}}^2}(\sigma_{22}+\sigma_{33})^2+\frac{1}{{S_{23}}^2}({\tau_{23}}^2-\sigma_{22}\sigma_{33})+\frac{1}{{S_{12=13}}^2}({\tau_{12}}^2+{\tau_{13}}^2)=1$$

$$(\sigma_{22}+\sigma_{33}<0) \qquad (16)$$

These criteria are here used to predict the failure of fibres and matrix, while the Choi-Chang's criterion is used to predict the onset of delamination, because it always give accurate estimations, as shown by many papers. According to the Choi-Chang's criterion delamination is predicted to start if $e_d^2>1$:

$$e_d^2 = D_a\left[\frac{\bar{\sigma}_{yz}^{\,n}}{S_i^n}+\frac{\bar{\sigma}_{xz}^{\,n+1}}{S_i^{n+1}}+\frac{\bar{\sigma}_{yy}^{\,n+1}}{Y_i^{n+1}}\right]^2 \qquad (17)$$

where $Y^{n+1}=Y_t^{n+1}$ if $\bar{\sigma}_{yy}\geq 0$, or $Y^{n+1}=Y_c^{n+1}$ if $\bar{\sigma}_{yy}<0$ (*t*=traction, *c*=compression), D_a is an empirical constant that is set after consideration of the material properties, $\bar{\sigma}_{ij}$ is the average stress at the interface between the n^{th} ply and the $n+1^{\text{th}}$ ply

$$\bar{\sigma}_{ij}^{\,n+1}=\frac{1}{h_{n+1}}\int_{t_{n-1}}^{t_n}\sigma_{ij}\,dt \qquad (18)$$

and *i* represents the in-situ strengths. It could be noticed that this delamination criterion disregards the transverse interlaminar stress σ_{33}. However numerical test carried out with criteria that considers this contribution [31] have shown it to be not relevant in the majority of cases.

The growth of delamination is simulated using a mesoscale model, though it is a common opinion that the most accurate description is provided either by fracture mechanics or cohesive zone models. The reason for this choice is that the mesoscale models should be equally accurate and, moreover, they offer the advantage that the progressive damage analysis can be carried out with a conventional, computationally efficient plate model. Indeed, these models provide a modified expression of the strain energy where the effects of damage are accounted by coefficients called the "damage indicators" that are computed apart once at a time, which represent the homogenized result of damage micromodels.

Using a mesoscale model, the effects of local failure mechanisms are accounted for by replacing the discretely damaged medium with an equivalent continuous and

homogeneous medium., which from an energy standpoint is equivalent to the damage micromodel. The displacement, strain and stress fields representing the exact microsolution in presence of delamination S^M are represented as the sum of the solution with the damage removed $\tilde{S}$ and the solution $\bar{S}$ of a residual problem where each cracked area, whose normal vector is $\underline{n}$, is loaded by the residual stress $\underline{n}\,\tilde{\sigma}$, i.e. $S^M = \tilde{S} + \bar{S}$. The damage indicators are defined as the integral of the strain energy for each elementary residual problem and just depend on the elastic properties. The solution of each residual problem can be obtained in analytic form [23], or via finite elements [24]. The homogenization must be carried out for any stacking sequence and for any kind of microdamage state. In the present paper, the homogenization is carried out apart from the simulation of the impact problem, using a 3D finite element discretization where delamination at specific interfaces is considered.

In summary, the homogeneization process is carried out as follows. On the mesoscale, the plies and the interfaces are homogenized to arrive at a continuum damage mechanics approach which derives from the theoretical and experimental works carried out in micromechanics [23,24]. The behavior of laminates is described through two mesocontituents, the single layer and the interface, which represent the thin layer of matrix between two adjacent plies. Under in-plane loading, the residual problem is solved assuming that the solution near an interface depends only on the state of damage of the interface. Under out-of-plane loading and whenever the interlaminar stresses are not negligible, i.e. the damage state of a ply depends on the state of damage of the adjacent plies, 3-D modeling is be used. The homogeneization of the interface is carried applying the three interlaminar stresses $\tilde{\sigma}_{13}$, $\tilde{\sigma}_{23}$, $\tilde{\sigma}_{33}$ simultaneously and assuming the strain energy stored in the interface under this loading as the energy reference. The residual solution is expressed as the sum of the three elementary solutions $\bar{\sigma}_{13}$, $\bar{\sigma}_{23}$, $\bar{\sigma}_{33}$ in the orthotropic basis of the interface. The damage variables (transverse cracking rate and delamination ratios of the interfaces) are assumed constant across the thickness of each mesoconstituent, but can vary changing the mesoconstituent. The damage state of each mesoconstituent is quantified by damage variables linked to the loss of stiffness of the mesoconstituent, whose evolution depends on damage forces that represent the variation of the energy with respect to the damage.

As final result, the strain energy is determined through damage indicators that are defined as the integrals of the strain energy for any basic residual problem. The strain

energy E_p^j of the interface γ_j is expressed as:

$$\frac{2E_p^j}{|\gamma_j|} = -\frac{(1+\bar{I}^1)\tilde{\sigma}_{13}}{\tilde{k}_1} - \frac{(1+\bar{I}^2)\tilde{\sigma}_{23}}{\tilde{k}_2} - \frac{(1+\bar{I}^3)\tilde{\sigma}_{33}}{\tilde{k}_3} \tag{28}$$

where $\tilde{k}_1$, $\tilde{k}_2$ and $\tilde{k}_3$ are the elastic stiffness coefficients of the interface, $\bar{I}^1$, $\bar{I}^2$ and $\bar{I}^3$ are the three damage indicators defined as the integral of the strain energy over the interface for each elementary problem. In order to carry out the homogeneization process through finite element computations, a cell subjected to the residual stresses is discretized by brick elements [59], as suggested in [23, 24]. The progressive failure analysis is carried out at each increment of displacement or loading by evaluating the homogeneized stresses at any point and comparing them to the strength. The comparison is made with the longitudinal or the shear strength, respectively, when ply failure or delamination are investigated. Delamination rises at the points where the interfacial shear stresses reaches the ultimate shear stress. A pre-existing delamination is extended to the points where the ultimate stress is reached. The procedure is continued till a given displacement or stress, the complete failure of the interface, or till the end of the contact time.

Numerical applications

The focal point being the assessment of the model for predicting rise and growth of delamination, as the thermo-structural model was already successfully tested in [49], impact problems published in the literature are retaken and solved with the structural and damage models described above. The aim is to show that a damage analysis carried out with SEUPT and the mesoscale model can be a fast and accurate alternative to use of 3-D FEA, fracture mechanics and other approaches currently used.

As the modelling of the contact force was already successfully assessed in [31], the load and displacement time histories are discussed and compared to the reference solution just in the first sample case. In this and in the successive cases, the damage predicted by the present modelling approach is compared to the results by other researchers and to experiments. Applications are presented to reference sample cases taken from the literature where delamination under impact loading is considered. The effects of simultaneously acting impact and thermal loading not still considered in the reference papers are analysed using the present model. Its capability of predicting thermally induced delaminations is assessed considering a thermo-elastic delamination problem which was previously investigated using a thermo-elastic interface model.

Case A: rectangular plate under impact loading

Consider a rectangular plate of size 100 x 75 x 1 mm made of 8 layers with the same properties and a $[45/-45/90/0]_s$ lay-up, which is impacted at the centre by an impactor of mass 0.412 Kg, an energy of 3.11 J and a spherical TUP of diameter 12.7 mm. The material properties for this sample case, which was formerly investigated by Iannucci [60], are reported in Table 1 (E_3, $G13$, G_{23}, υ_{13}, υ_{23}, Z_T, Z_C, S_{13}, S_{23} are assumed, as they are not reported in [60]). As customary, the symbols E_1, E_2, E_3 represent the elastic moduli, G_{12},G_{13}, G_{23} the in-plane and transverse shear moduli, υ_{12}, υ_{13}, υ_{23} the Poisson's ratios, while X_T, X_C, Y_T, Y_C, Z_T, Z_C indicate tensile (T) and compressive (C) strengths in the longitudinal and transverse directions and S_{12}, S_{13}, S_{23} represent the in-plane and transverse shear strengths, 1 being the direction of fibres and 2,3 the directions transverse to it.

In the reference paper by Iannucci, the analysis was carried out using solid-shell and interface elements for modeling the plate and solid elements for modeling the impactor. The plate was assumed to be simply-supported at the bound. Stress based criteria were used in for predicting the failure of fibres and matrix, while an interface model coupled with an energy based criterion was used for predicting delamination. Iannucci considered a discretization into 53,946 nodes, where 16,200 elements were used for modeling the laminated plate together with 8,100 interface elements and 19,728 solid elements were used for the impactor.

Table 1. Elastic moduli, strengths and thermal properties for the rectangular plate subject to impact loading (Case A).

E_1 [GPa]	E_2 [GPa]	E_3 [GPa]	G_{12} [GPa]	G_{13} [GPa]	G_{23} [GPa]	υ_{12}	υ_{13}	υ_{23}
140.0	9.5	9.5	5.8	5.8	5.8	0.3	0.3	0.3
X_T [MPa]	X_C [MPa]	Y_T [MPa]	Y_C [MPa]	Z_T [MPa]	Z_C [MPa]	S_{12} [MPa]	S_{13} [MPa]	S_{23} [MPa]
2000	1650	70	240	70	240	105	85	105
k_{11} [W/mK]	k_{22} [W/mK]	k_{33} [W/mK]	α_{11} [$10^{-6}K^{-1}$]	α_{22} [$10^{-6}K^{-1}$]	α_{11} [$10^{-6}K^{-1}$]			density [Kg/m^3]
13	1.7	1.7	-0.8	28	28			1540

The simulation by the present model was carried out using the same in-plane discretization of [60], because the results may be mesh dependent. A uniform subdivision into 40 elements was considered across the thickness in order to carry out the homogeneization around the delaminated area. Extent and position of the damaged area were initially approximated with the FEA analysis by SEUPT and successively refined substituting the results by the solid model into the plane model. Just two steps were carried out, as the results did not significantly change in the successive steps. This analysis by solid elements was carried out just at the interface between the layers at 45° and -45° close to the upper face, since according to [60] initiation and propagation of delamination were supposed to occur along this plane, but all the interfaces between the layers could be considered, either separately or together. Like in [60], the response to failure was supposed to be elastic, though this could be unrealistic in certain cases, while the effects of damping, strain-rate and microcracks were disregarded.

As the mesoscale model represents the effects of the damage mechanisms involving the interface resin film, it is expected that the present analysis may give results equivalent to those of the interface model applied in [60].

The results for this case are presented in Figures 1 to 3.

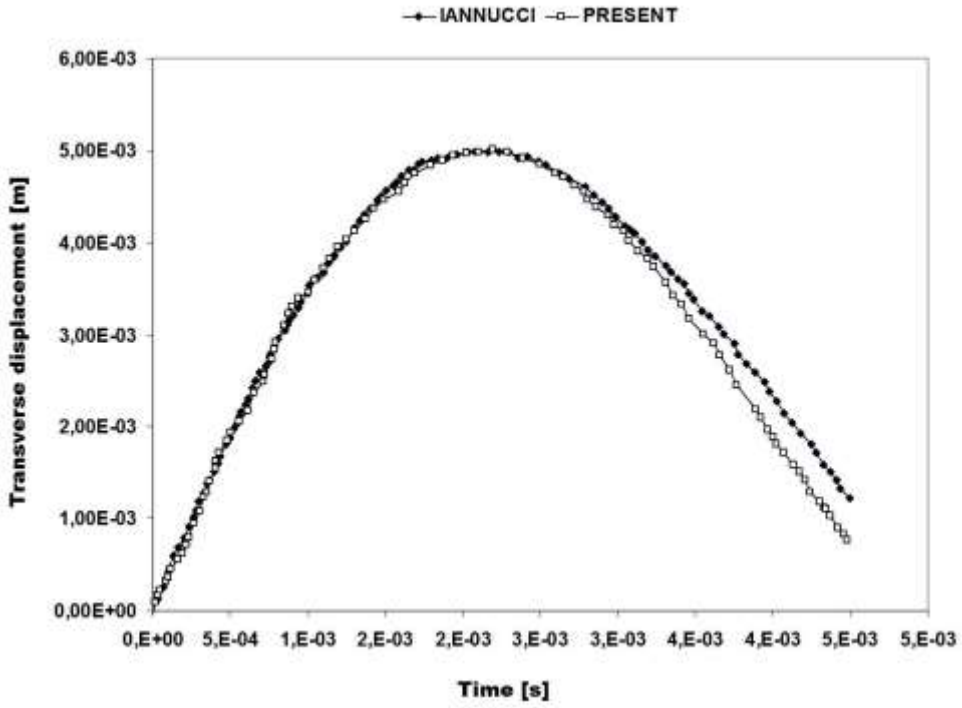

Figure 1. Transverse displacement time history curves for the $[45/-45/90/0]_s$ CFRP rectangular plate under impact loading of Case A. Reference results by Iannucci [60] are for a length-to-thickness ratio S of 100.

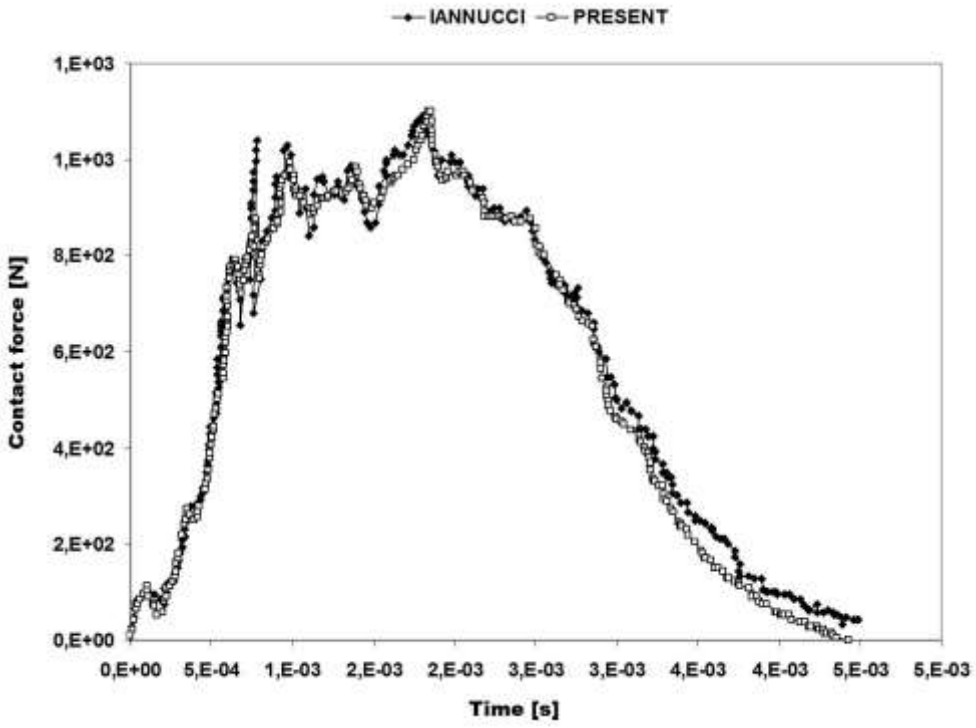

Figure 2. Contact force time history curves for the CFRP rectangular plate under impact loading of Case A, with a length-to-thickness ratio S of 100

.

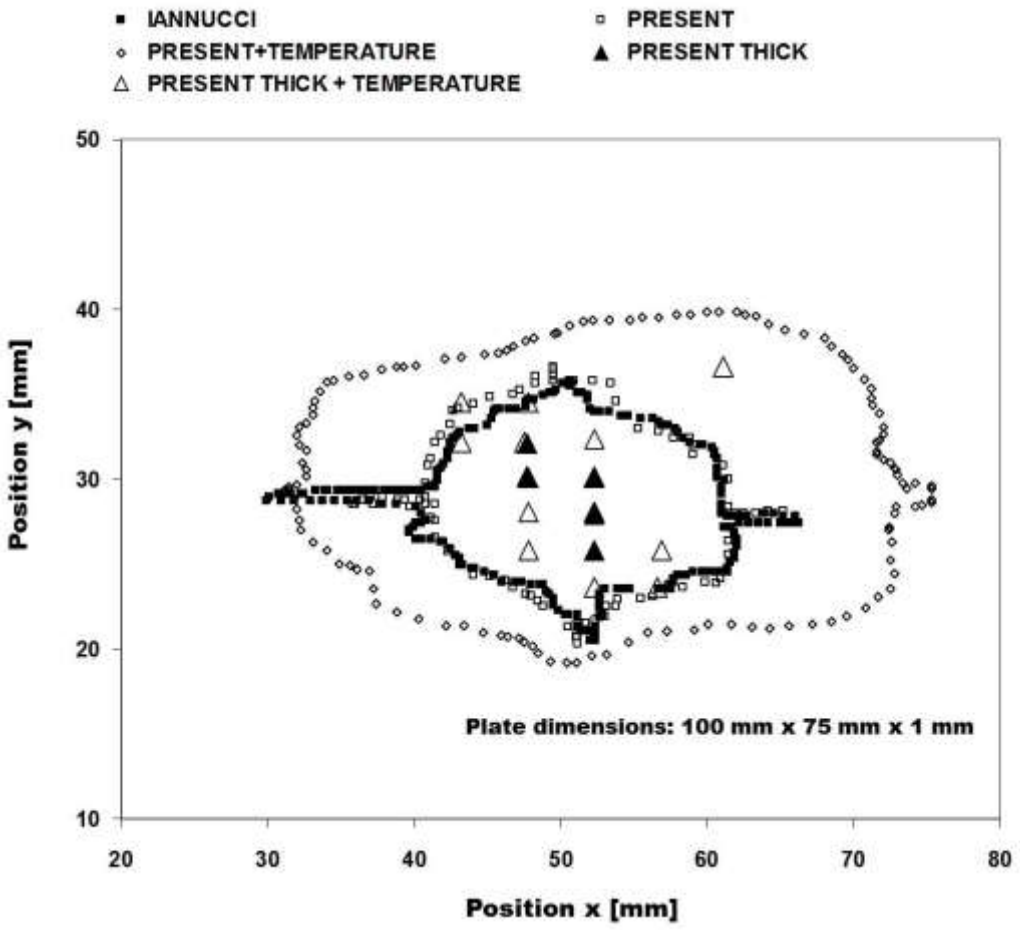

Figure 3. Delamination failure envelopes for the CFRP rectangular plate under impact loading of Case A with S=100. Additional results are given for a thick case with S=3 and temperature gradients (sinusoidal distributed temperature with amplitude of 125 °C at the upper face and 25 °C at the lower face).

Figure 1 gives the transverse displacement time history curves predicted by the present analysis and that by Iannucci, Figure 2 represents the comparison of the contact force time history curves, while Figure 3 represents the delamination failure envelopes. It may be observed that small discrepancies start to appear at the end of the contact time. It is believed that they are due to the partial capability of the models to account for the interaction between the failure mechanism, as a consequence of the constraints to the CPU time. Indeed, examples taken from the literature have shown a similar reciprocal behavior of models, with larger discrepancies with respect to experiments as the time unfolds. However, at the end of the contact time the actual result appear in a much better agreement with experiments than the reference results. The effects of a sinusoidal distributed temperature, which has an amplitude of 125 °C at the upper face and of 25 °C at the lower face are also reported in Figure 3. The thermal properties assumed in the computations are given at the end of Table 1. As shown by Figure 3, the stresses induced

by the temperature gradients add to those due to the impact loading, resulting into an enlarged delamination area.
The temperature profile across the thickness predicted by the present temperature thermal model is reported in Figure 4. As the plate considered by Iannucci is rather thin, the temperature variation across the thickness is linear.
A thicker case was considered in order to show the capability of the present model to capture the variation of the temperature irrespective for the thickness and the different behavior of thin and thick cases under impact loading. The results for a length-to-thickness ratio of 3 are reported in Figure 5, which put in evidence that the temperature distribution is no longer linear and that the extension of the delaminated area is the result of a less pronounced bending and the rise of thermal stresses.
The results show that the displacement and force time history curves and the delamination failure envelopes by the present model are in a good agreement with those of the reference paper [60], so it is concluded that the present approach can be used as an alternative to 3-D models and fracture mechanics or interface models.

Summing up, the analysis was initially carried out with relatively inexpensive standard plate elements, whose predictions were locally updated around the impact area using SEUPT at some time steps. Few seconds are required for each applications of SEUPT carrying out the computations on a laptop computer. The homogeneization procedure by the mesoscale model was carried out once at a time in some minutes by a symbolic calculus tool, then each of the successive applications required only few seconds. As a result, few minutes are required for the overall simulation process. The degree of accuracy of results can be improved suitably choosing the number and the length of the single time steps, the number of iterations of SEUPT, the extent of the region where updating is carried out and the meshing of PFA, i.e. the initial analysis whose results are updated by SEUPT.
Other sample cases are considered hereafter, in order to assess whether the previous conclusions still hold.

Case B: square plate under multiple impact loading

The delamination damage of a laminated plate clamped at its edges, subject to simultaneous impacts by cylindrical impactors was investigated by Chakraborty [25]. A

square plate with sides 7.62 cm long, a thickness of 0.254 mm, made of 16 graphite/epoxy plies with the properties reported in Table 2 and a $[0/-45/45/90]_{2S}$ was considered (some material data were assumed, being not given in [25]). The analysis was carried out with 20 x 20 x 2 solid elements, respectively in the in-plane directions and across the thickness. Two impactors striking at symmetrical locations were considered, with a diameter of 5 mm and a length of 20 mm, which impacted the plate with a delay of 25, 50 and 100 μs and a velocity of 9 m/s. The impact points were located

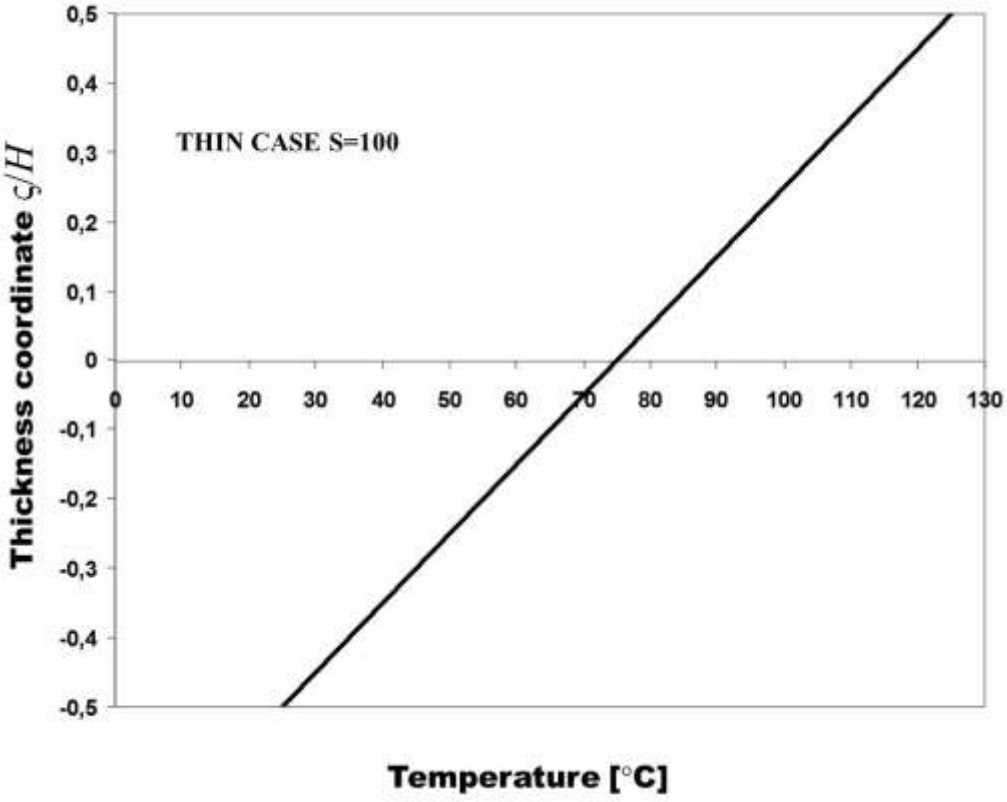

Figure 4. Temperature profile across the thickness, for the plate of Case A with a length-to-thickness ratio S=100 and sinusoidal distribution of temperature with amplitude 125 °C at the upper face and 25 °C at the lower face (centre of the plate).

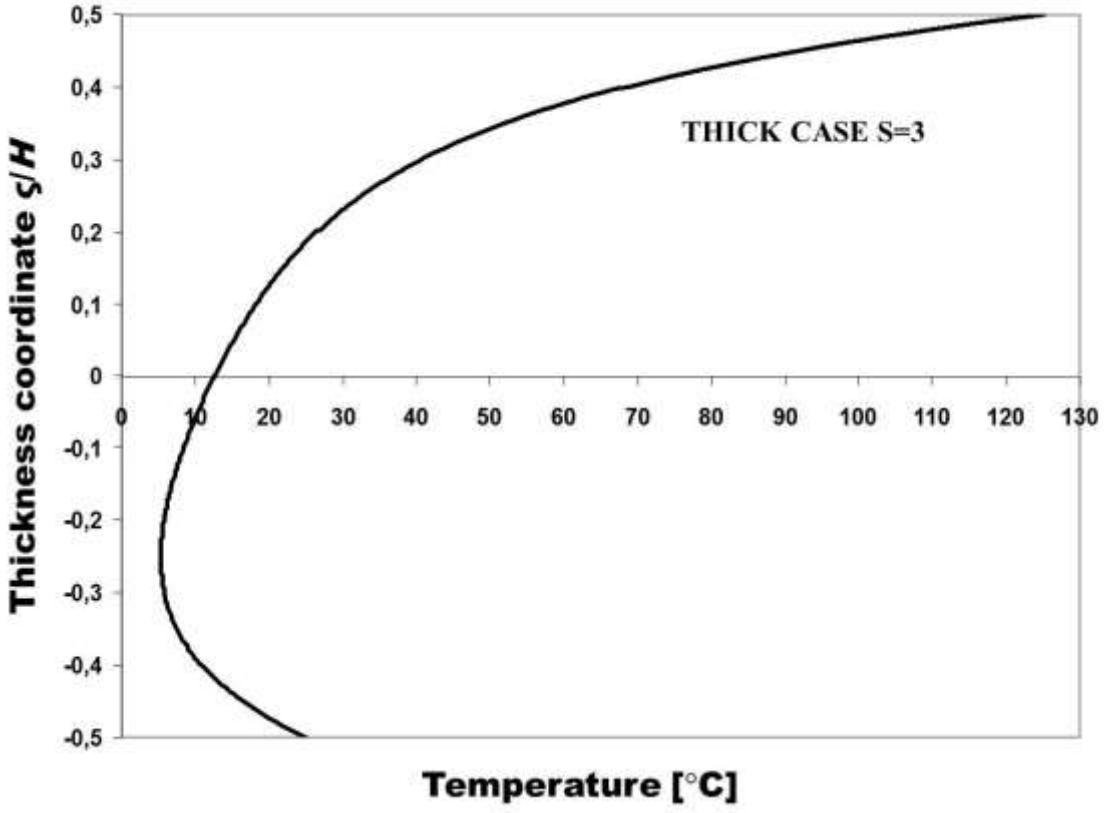

Figure 5. Temperature profile across the thickness, for the plate of Case A with a length-to-thickness ratio S=3 and sinusoidal distribution of temperature with amplitude 125 °C at the upper face and 25 °C at the lower face (centre of the plate).

respectively at x=1.905 cm, y=3.81 cm and x=5.715 cm, y=3.81 cm, the coordinate system being assumed at the centre of the plate. The distribution of the pressure over the contact area was assumed as Hertzian, with a uniform distribution along the length, but assuming the cylinders slightly barreled to reduce the stress concentration at the ends. The effects of the second impactor on the overall loading are taken into account once it strikes the plate. Delaminations at the interfaces were computed using the Choi-Chang's criterion averaging the stresses at the interfaces.

The results by the present model are compared to those by Chakraborty in Figures 6 to 8. As the reference results show the damage at any interface, the capability of the present model to predict the damage at any point across the thickness can be assessed. The results reported refer to an interval of time between the two successive impacts of 50 μs. The same in-plane discretization into 20 x 20 elements as in [25] was adopted in order to compare results not affected by errors due to different mesh size. Figure 6 shows the delaminated area at the first interface from the upper face, while Figures 7 and 8 refer to the successive two interfaces. It could be noticed that the accuracy of the present model is

comparable to that of the 3-D model of [25], as the results are in a good agreement at all the points. In order to have an assessment of the computational time, the same problem was discretized by the solid elements used in the homogeneization procedure. The analysis required about four minutes on a laptop computer, while the present model with SEUPT required less than half the time and a lower memory storage occupation. Results with the same accuracy of Figures 6 to 8 were obtained for time intervals of 25 and 100 μs, which are not reported here to contain the length of the paper.

Table 2. Material properties for the rectangular plate subject to multiple impact loading (Case B).

E_1 [GPa]	E_2 [GPa]	E_3 [GPa]	G_{12} [GPa]	G_{13} [GPa]	G_{23} [GPa]	υ_{12}	υ_{13}	υ_{23}
145.4	9.99	9.99	5.69	5.69	5.69	0.3	0.3	0.3
X_T [MPa]	X_C [MPa]	Y_T [MPa]	Y_C [MPa]	Z_T [MPa]	Z_C [MPa]	S_{12} [MPa]	S_{13} [MPa]	S_{23} [MPa]
1778	1731	55.2	294	55.2	294	101.2	101.2	101.2
k_{11} [W/mK]	k_{22} [W/mK]	k_{33} [W/mK]	α_{11} [$10^{-6}K^{-1}$]	α_{22} [$10^{-6}K^{-1}$]	α_{11} [$10^{-6}K^{-1}$]			density [Kg/m^3]
13	1.7	1.7	-0.8	28	28			1535.68

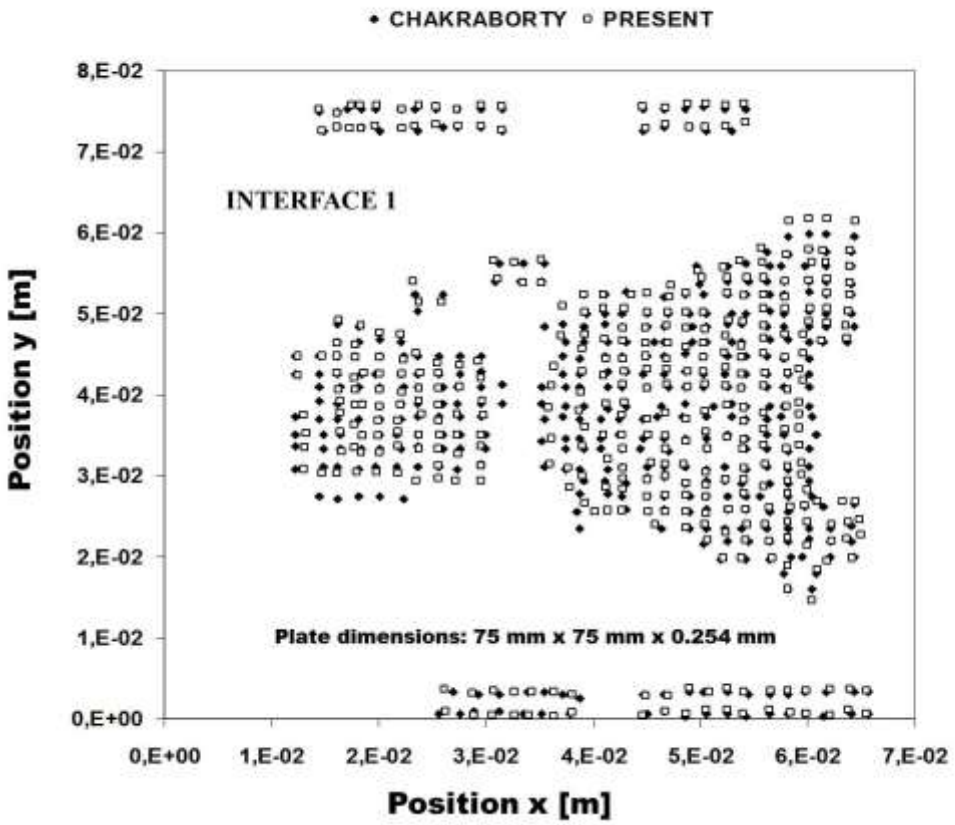

Figure 6. Delaminated area at the first interface from the upper face of the $[0/-45/45/90]_{2S}$ CFRP square plate with clamped edges and length-to-thickness ratio S=300 of Case B, subject to multiple impact loading (reference results from [25]).

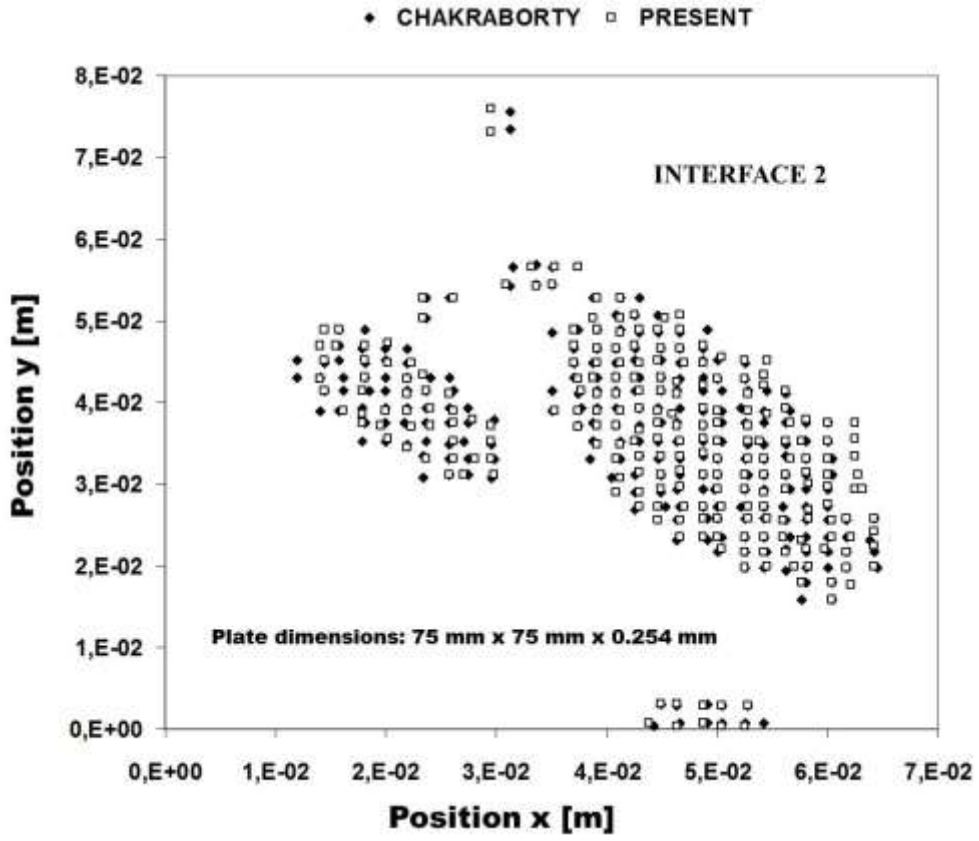

Figure 7. Delaminated area at the second interface from the upper face of the CFRP square plate with clamped edges of Case B subject to multiple impact loading.

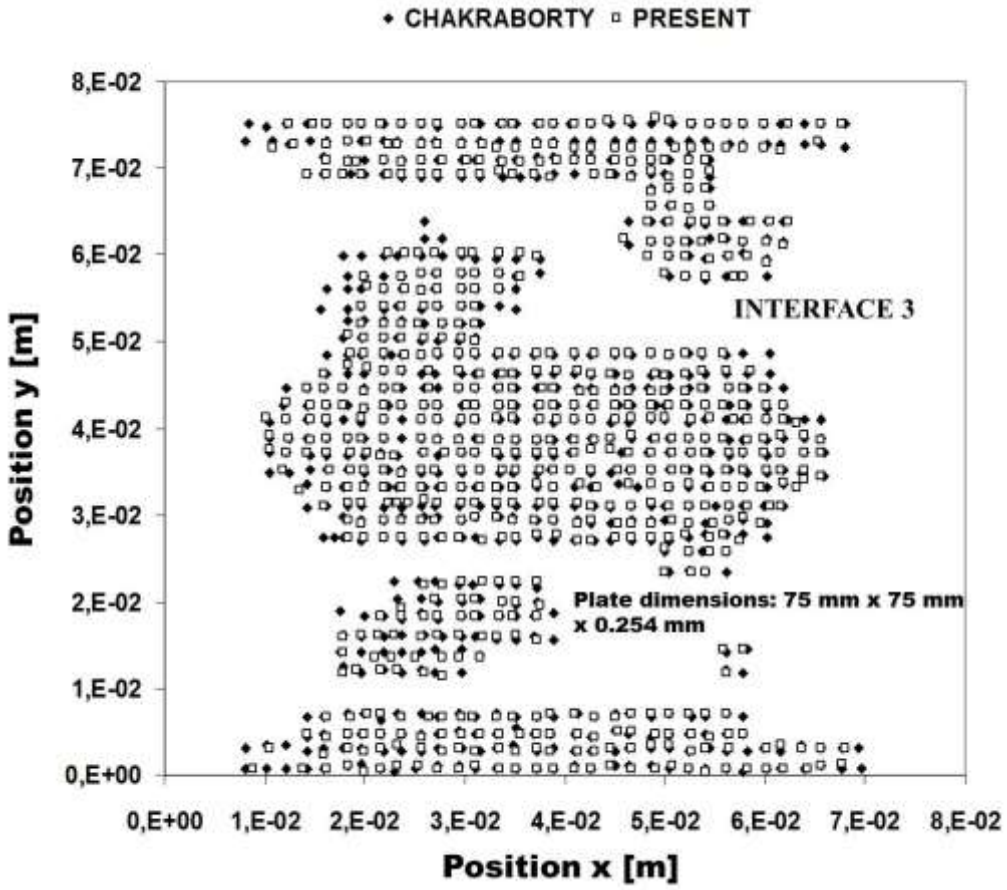

Figure 8. Delaminated area at the third interface from the upper face of the CFRP square plate with clamped edges subject to multiple impact loading of Case B.

The combined effects of thermal and impact loading are shown in Figure 9. The results refer to the region at the second interface with x ranging from 0.01 to 0.035 m and y ranging from 0.03 to 0.05 m. As the plate is thin and the constituent plies are made of the same material, the temperature profile is linear across the thickness. The results show an enlarged delaminated area because the thermally induced stresses are superposed to those induced by the impact loading. Also in this case, the temperature is assumed to be sinusoidal, with an amplitude of 125 °C at the upper face and of 25 °C at the lower face. The result corresponding to a length-to-thickness ratio of 3 is reported in Figure 10. In this thick case, the temperature profile is no longer linear, as shown by Figure 11. The delamination damage, which is less extended than in the thin case, is the result of a smaller bending deformation, as the thickness is increased, and of larger temperature gradients across the thickness.

As shown by the comparison with the reference results obtained with 3-D FEA, the present models is able to capture the delamination damage at all the points in the volume, requiring a low computational effort. Further accuracy test are presented hereafter.

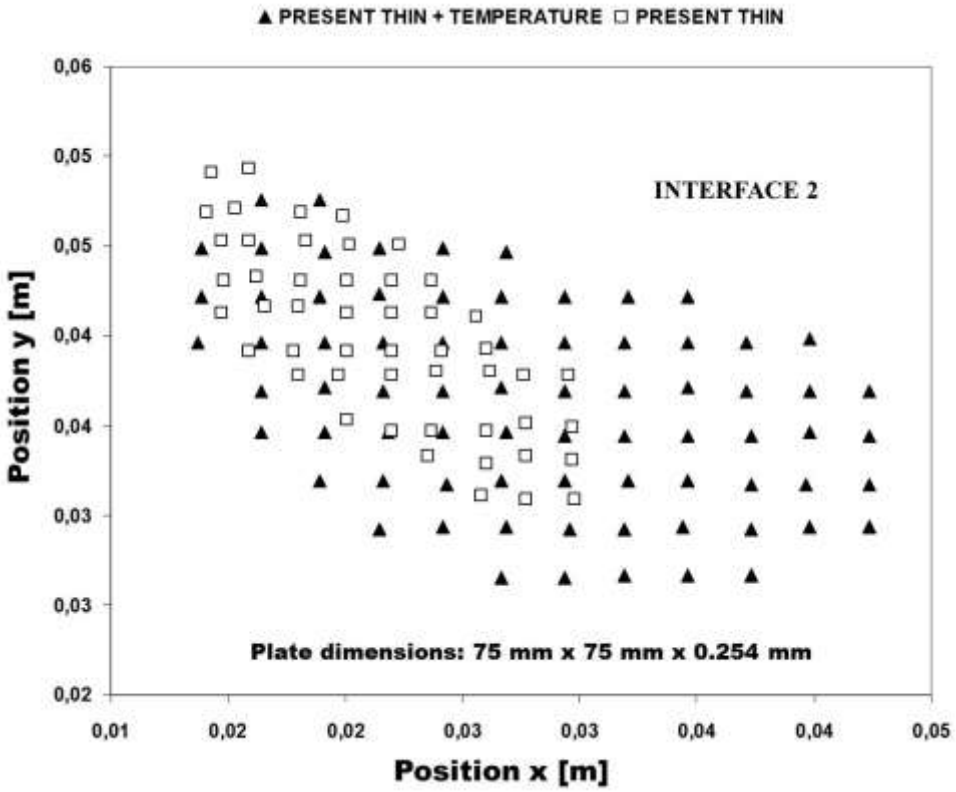

Figure 9. Delamination failure envelopes at x=0.01-0.035 m, y=0.03-0.05 m, for the CFRP clamped plate under multiple impact loading of Case B, with a length-to-thickness ratio S=300 and with/without sinusoidal distributed temperature (amplitude of 125 °C at the upper face and 25 °C at the lower face).

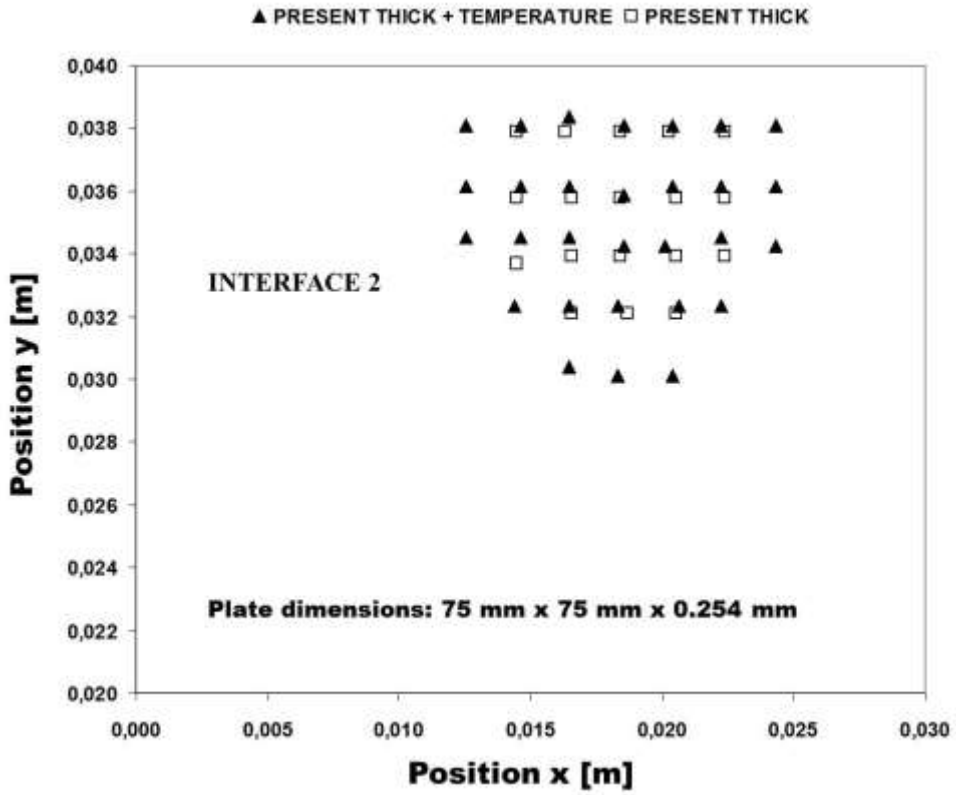

Figure 10. Delamination failure envelopes at x=0.01-0.035 m, y=0.03-0.05 m, for the CFRP clamped plate under multiple impact loading of Case B with a length-to-thickness ratio S=3 and with/without sinusoidal distributed temperature (amplitude of 125 °C at the upper face and 25 °C at the lower face).

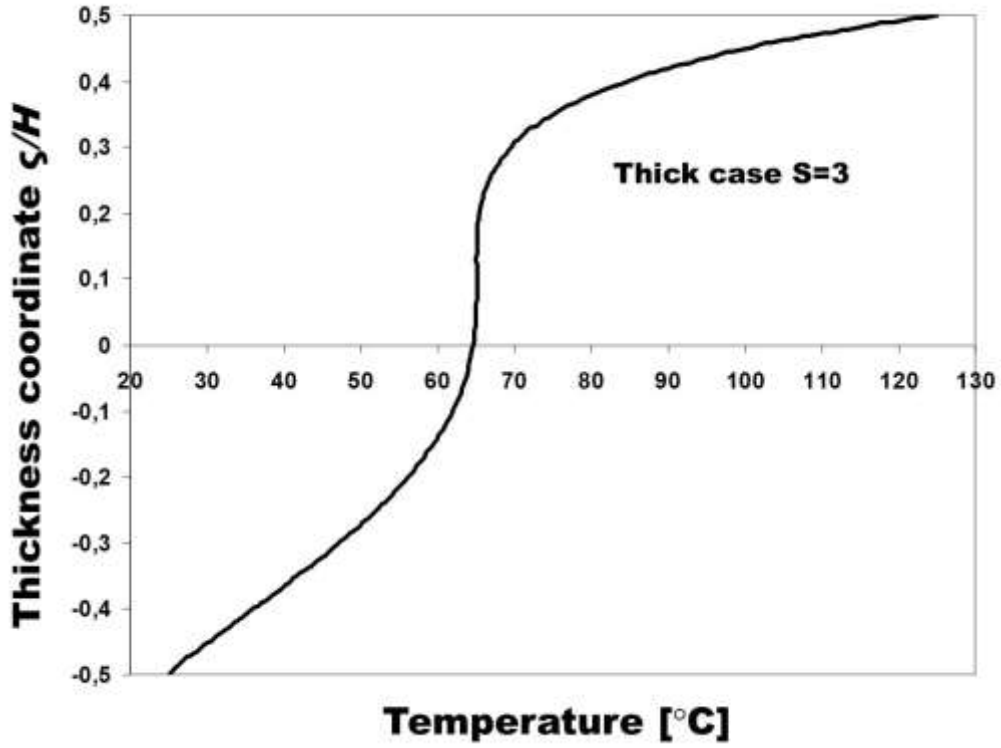

Figure 11. Temperature distribution across the thickness for the CFRP clamped plate under multiple impact loading of Case B. Length-to-thickness ratio S=3, sinusoidal temperature distribution of amplitude 125 °C at the upper face and 25 °C at the lower face (centre of the plate).

Case C: comparison with experimental results

A $[0_4/90]_s$ square plate with 200 mm sides and 1.25 mm thick is now considered, which is impacted by an impactor of mass 1.5 Kg and a hemispherical end with diameter 7 mm . The plate is sustained by a supporting plate with an open hole of diameter 35 mm at its centre, so it is simply supported on the edge of the hole. In this case, a comparison is made with the experimental results by Nishikawa et al. [61]. Ultrasonic scanning images of the impact induced delaminated area were presented for impactor energies of 1 to 3 J. Since during these low velocity impacts the contact time is long enough, thus the inertial effect is negligible, a static simulation was carried out with 3-D solid elements. A butter-fly shaped delamination was observed at the 90/0 lower interface, while the fracture of fibres was detected at the impact point and a long crack in the direction of fibres was detected in the unimpacted 0 ply at the lower surface. To simulate this crack at the lowermost ply, Dugdale cohesive elements were incorporated between the solid elements in [61].

The simulation by the present model was carried out considering inertial effects and the material properties of plies given in Table 3. The elastic properties were taken from [61], while the strength properties of plies and the density were assumed, as they were not

indicated in the reference paper because strength parameters of cohesive elements were provided. Just the case with the largest impact energy of 3 J was considered, as the damaged region has the same shape of lower energy impacts, but a larger extension. Figure 12 shows the comparison between the delamination area at the 90/0 lower interface predicted by the present model and that detected by ultrasonic scanning [61]. The origin of coordinates is assumed at the central point of the plate where impact loading is applied. It could be noticed that the present model gives accurate predictions also as compared to experiments, thus it can be used as an alternative with a lower computational effort, as discussed above, to customary models.
As a further assessment, next a sample problem were delamination is induced by thermal loading is considered.

Case D: delamination crack loaded by temperature gradient

The coupled thermo-mechanical delamination problem by Hattiangadi and Siegmund [48] is now solved using the present modeling approach. In the reference paper, unidirectional reinforced laminates of thickness H=2 mm and length L=30 mm with SiC fibres in Al_2O_3 matrix with initial delamination cracks were treated using a micromechanical approach based on a traction-separation law by a cohesive zone model. Bridged cracks of initial length 2a that was varied between a/H=2 to 6 were considered, which were positioned at H_1=0.211 H from the upper hot face. The temperature of the upper face was increased up to 1500 K, while the lower face was kept at the reference temperature of 300 K. The sides were insulated and the displacement boundary conditions were those of traction free laminates. The micro-mechanism based cohesive model was used to assess the contribution of bridging fibers to conductance and crack opening. The influence of critical mechanical and thermal parameters of the bridging zone was numerically assessed through a finite element analysis of the crack tip energy release rate (G_I, G_{II} and total G_T) and heat flux across the crack, assuming a linear variation of displacement and temperature jumps across the crack and a modified version of the crack closure integral. Plane quadrilateral elements were used for discretizing the problem across the thickness, a frictionless contact conditions was assumed over the crack surfaces and the radiative heat transfer between the crack surfaces was accounted. In this problem, the thermo-mechanical behavior around the crack determines the temperature distribution and, as a consequence, the loading of the crack. The results by

Table 3. Material properties for the square plate simply supported at the edge of a central circular region (Case C).

E_1 [GPa]	E_2 [GPa]	E_3 [GPa]	G_{12} [GPa]	G_{13} [GPa]	G_{23} [GPa]	υ_{12}	υ_{13}	υ_{23}
148	9.57	9.57	4.5	4.5	3.5	0.356	0.356	0.49
X_T [MPa]	X_C [MPa]	Y_T [MPa]	Y_C [MPa]	Z_T [MPa]	Z_C [MPa]	S_{12} [MPa]	S_{13} [MPa]	S_{23} [MPa]
1778	1731	55.2	294	55.2	294	101.2	101.2	101.2
density [Kg/m^3]								
1550								

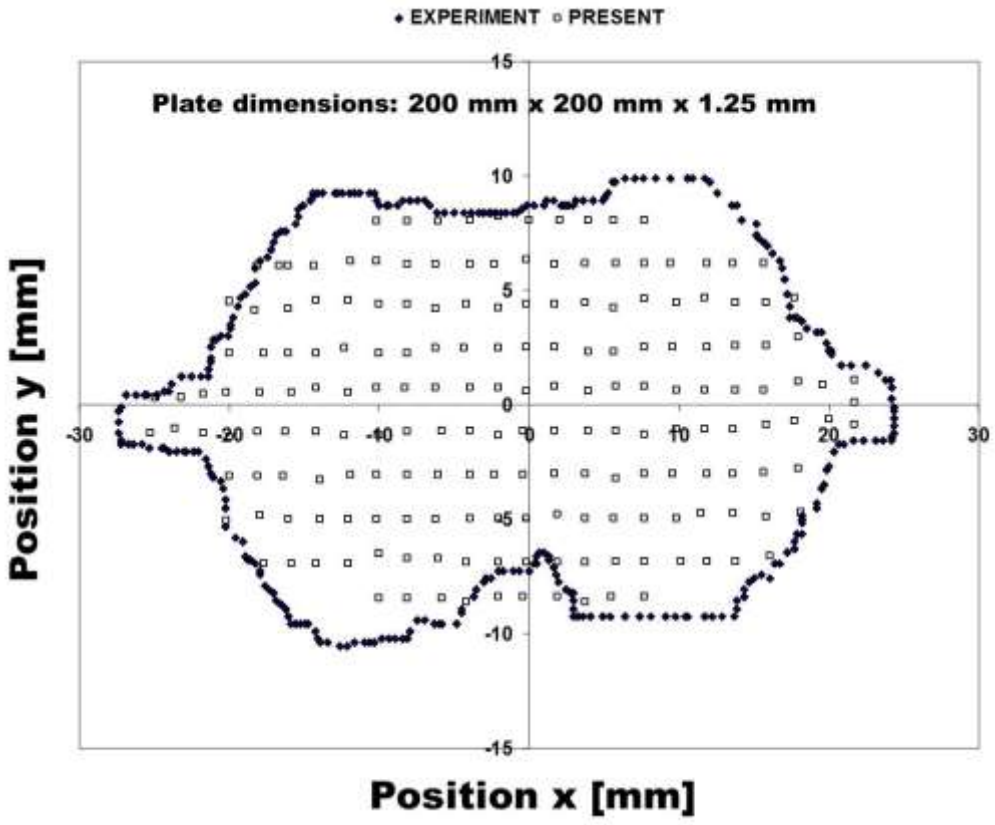

Figure 12. Comparison to experimental results for a $[0_4/90]_s$ CFRP square plate sustained by a supporting plate with an open hole at the centre, subject to impact loading of Case C: delaminated area at the 90/0 lower interface (experimental results from [61]).

Hattiangadi and Siegmund [48] show that increasing the temperature jump from top and bottom faces , the differences of the thermal expansion due to the crack initially lead to bending of the laminate. A large fraction of the conductance of the undamaged laminate is recovered initially, but increasing the temperature jump the heat flux across the crack can be sustained only by the shorter crack. The short crack is a nearly perfectly conducting crack, while the longer cracks show a transition to a nearly insulating behavior at large values of applied temperature difference from top to bottom. At high temperature, a condition of breackdown in thermal shielding is shown, where the problem is dominated by radiation. As the heat flux breaks down, the crack becomes insulating, buckling delamination starts and the rate of increase in G_T rises substantially.

Table 4. Temperature at the onset of buckling delamination for the unidirectional laminate with SiC fibres in Al_2O_3 matrix, varying the crack length (Case D).

Temperature [K]	Crack length			
	a/H=3.0	*a/H*=3.5	*a/H*=4.0	*a/H*=6.0
Present	969	782	644	541
Ref. [48]	976	784	639	535

Table 5. Meterial properties for the cracked unidirectional laminate with SiC fibres in Al_2O_3 matrix, under temperature gradient (Case D).

Temp [K]	E_T [GPa]	E_L [GPa]	G_T [GPa]	G_L [GPa]	υ_T	υ_L	k_T [W/mK]	k_L [W/mK]	α_T [$10^{-6}K^{-1}$]	α_L [$10^{-6}K^{-1}$]
300	392.7	346.7	121.5	137.4	0.43	0.17	18.64	23.47	7.56	5.62
573	376.5	333.2	116.2	131.7	0.43	0.17	10.84	13.11	8.29	6.49
873	358.9	318.8	110.0	125.4	0.43	0.17	7.91	9.07	8.67	7.1
1500	324.3	289.1	98.8	112.9	0.43	0.18	5.68	5.92	8.89	7.48

The present results are reported in Table 4 while the material properties are reported in Table 5. The results show the temperature jumps at the onset of buckling delamination predicted by the present thermo-structural model for crack lengths *a/H* of 3.0-3.5-4.0 and 6.0. A finite element analysis of the problem was carried out by the mixed solid elements developed in [59], in order to perform the homogeneization by the mesoscale model, while the onset of buckling delamination was computed using SEUPT. As discussed above, the effects of cracks are brought into the model by the damage indicators that multiply the various contributions by strains and stresses to the strain energy. Only the regime till to the rise of buckling was considered, where the thermal loading is substantially sustained without a breakdown in thermal conductivity, because the present model does not currently account for the contribution of the radiative heat transfer. It could be noticed the very good agreement between the present and the reference results, due to the good correlation with the temperatures at the onset of buckling estimated from the paper by Hattiangadi and Siegmund [48]. This proves that quite accurate results can be obtained for thermo-elastic delamination problems using the mesoscale model and the zig-zag thermo-structural modell.

Concluding remarks

A thermo-mechanical delamination analysis was carried out using a recently developed refined plate model with adaptive representation of displacement and temperature and

fixed functional d.o.f. With the aim to adapt to the variation of solutions, the representation of displacements and temperature can be different from point to point across the thickness, though just the mid-plane displacements, the shear rotations and the temperatures at the upper and lower faces are chosen as functional d.o.f., in order to have the minimal number of variables. The transverse shear and normal stresses, the transverse normal stress gradient, the temperature and the heat flux are made continuous at the layer interfaces, as required for satisfying the equilibrium and fulfilling the heat conduction equation.

This model was chosen because it gives accurate results with a low computational effort. Indeed, previous applications have shown that though memory storage dimension and processing time is nearly equal to that of simplified models with the same d.o.f., the interlaminar stresses are computed with an accuracy comparable to that of discrete-layer models, though compared with these refined models the processing time is shorter and the number of functional d.o.f. is smaller.

To make the model even faster, the expressions of the continuity functions and the coefficients of hierarchic terms enabling the model to be adaptive are here determined once at a time using a symbolic calculus tool. In this paper, progressive delamination failure problems under thermo-mechanical loading were investigated with the aim to assess whether the present thermo-structural and damage models can be accurate compared to 3-D FEA. The onset of delamination is computed through stress based criteria, as customary with 2-D FEA, but instead of simulating the delamination growth degrading the elastic properties of the failed regions, here a mesoscale model is used. The strain energy updating technique by the author was employed to develop an efficient C° 2-D finite element model. The aim of this paper is to show that the damage analysis can be equally accurate but with a lower computational effort than 3-D FEA if carried out with SEUPT and a mesoscale model, instead of using fracture mechanics or cohesive interface models for describing the behavior of delamination cracks. Impact problems taken from the literature and a thermo-elastic delamination problem were solved with the purpose to assess the correct implementation and the accuracy of the damage model, then these impact problems were reconsidered under temperature fields.

The results show the good accuracy and the low computational cost of the present approach. In all the examined sample cases, a good agreement is shown with the results of 3-D FEA and of experiments. The mesoscale model efficiently accounts for the effects of the evolving damage without the need of guessing suited multiplication factors, as with the ply-discount theory. The analysis carried out with inexpensive standard plate elements,

whose predictions are updated around the impact area using SEUPT is quickly carried out. The homogeneization procedure by the mesoscale model being carried out apart with a symbolic calculus tool takes only few seconds in any application. The degree of accuracy can be improved choosing the number and the length of the single time steps, the number of iterations of SEUPT and the extent of the region where updating is carried out.

References

1. C.C. Foo, G.B. Chai and L.K. Sea, A Model to Predict Low-Velocity Impact Response and Damage in Sandwich Composites, *Composites Sci. & Technology*, vol. 68, pp. 1348–1356, 2008.

2. V. Tita, J. de Carvalho and D. Vandepitte, Failure Analysis of Low Velocity Impact on Thin Composite Laminates: Experimental and Numerical Approaches, *Compos. Structures*, vol. 83, pp. 413–428, 2008.

3. T.E. Tay, G. Liu, V.B.C. Tan, X.S. Sun and D.C. Pham, Progressive Failure Analysis of Composite, *J. Compos. Materials*, vol. 42, pp. 1921-1966, 2008.

4. M.R. Garnich and M.K. Akula Venkata, Review of Degradation Models for Progressive Failure Analysis of Fiber Reinforced Polymer Composites, *Appl. Mech. Rev*iews, vol. 62, pp. 1-35, 2009.

5. P.F. Liu and J.Y. Zheng, *Review on Methodologies of Progressive Failure Analysis of Composite Laminates*, in *Continuum mechanics*, A. Koppel, and J. Oja Ed. New York: Nova Science Publishers, 2009.

6. A. Faggiani and B.G. Falzon, Predicting Low-Velocity Impact Damage on a Stiffened Composite Panel, *Composites: Part A*, vol. 41, pp. 737-749, 2010.

7. V.V. Bolotin, Delaminations in Composite Structures: Its Origin, Buckling, Growth and Stability. *Composites: Part B*, vol. 27, pp. 129-145, 1996.

8. P.P. Camanho, F.L. Matthews, Delamination Onset Prediction in Mechanically Fastened Joints in Composite Laminates. *J. Compos. Materials*, vol. 33, pp.906-927, 1999.

9. N.S. Choi, A.J. Kinloch and J.G. Williams, Delamination Fracture of Multidirectional Carbon Fiber/Epoxy Composites Under Mode I, Mode II and Mixed Mode I/II Loading. *J Compos. Materials*, vol. 33, pp. 73-100, 1999.

10. P.F. Lee, S.J. Hou, J.K. Chu, X.Y. Hu, Y.L. Liu, J.Y. Zheng, A. Zhao and L. Yan, Finite Element Analysis of Postbuckling and Delamination of Composite Laminates Using Virtual Crack Closure Technique, *Composite Structures*, vol. 93, pp. 1549-1560,

2011.

11. R. de Borst and J.J.C. Remmers, Computational Modelling of Delamination, *Composites Sci. & Technology*, vol. 66, pp. 713-722, 2006.

12. N.D. Flesher and C.T. Herakovich, Predicting Delamination in Composite Structures, *Composites Sci. & Technology*, vol. 66, pp. 745-754, 2006.

13. G.A.O Davies, D. Hitchings and J. Ankersen, Predicting Delamination and Debonding in Modern aerospace Composite Structures. *Composites Sci & Technology*, Vol. 66: 846-854, 2006.

14. D.J. Elder, R.S. Thomson, M.Q. Nguyen and M.L. Scott, Review of Delamination Predictive Methods for Low Speed Impact of Composite Laminates, *Composite Structures*, vol. 66, pp.677-683, 2004.

15. J. Wang and B.L. Karihaloo, Multiple Cracking in Angle-Ply Composite Laminates, *J. Compos. Materials*, vol. 29, pp. 1321-1336, 1995.

16. V.N. Bulsara, R., Talreja and J. Qu, Damage Initiation Under Transverse Laoding of Unidirectional Composites with Arbitrarily Distributed Fibers, *Compos. Sci. & Technology*, vol. 59, pp. 673-682, 1999.

17. I.M., Daniel and O. Ishai, *Engineering Mechanics of Composite Materials* 2nd Edition, Oxford University Press, 2005.

18. J-M. Berthelot, Transverse Cracking and Delamination in Cross-Ply Glass-Fiber and Carbon-Fiber Reinforced Plastic Laminates: Static and Fatigue Loading, *Appl. Mech. Reviews*, vol. 56, pp. 111-147, 2003.

19. V. La Saponara, H. Muliana, R. Haj-Ali and G.A. Kardomateas, Experimental and Numerical Analysis of Delamination Growth in Double Cantilever Laminated Beams, *Eng. Fracture Mechanics*, vol. 69, pp. 687-699, 2002.

20. R. Borg, L. Nilsson and K. Simonsson, Simulation of Low Velocity Impact on Fiber Laminates Using a Cohesive Zone Based Delamination Model, *Compos. Sci & Technology*, vol. 64: 279-288, 2004.

21. M. Nishikawa, T. Okabe and N. Takeda, Numerical Simulation of Interlaminar Damage Propagation in CFRP Cross-ply Laminates Under Transverse Loading. *Int. J. of Solids & Structures*, vol. 44, pp.3101-3113, 2007.

22. R.G. Wang, L. Zhang, W.B. Liu and X.D. He, Numerical Analysis of Delamination Buckling and Growth in Slender Laminated Composites Using Cohesive Element Method, *Computational Materials Science*, vol. 50, pp. 20-31, 2010.

23. P. Ladevèze and G. Lubineau, On a Damage Mesomodel for Laminates: Micromechanics Basis and Improvement, *Mech. of Materials*, vol. 35, pp. 763-775, 2003.

24. P. Ladevèze, G. Lubineau and D. Marsal, Towards a Bridge Between the Micro- and Mesomechanics of Delamination for Laminated Composites, *Composites Sci. & Technology*, vol. 66, pp. 698-712, 2006.

25. D. Chakraborty, Delamination of Laminated Fiber Reinforced Plastic Composites Under Multiple Cylindrical Impact, *Materials & Design*, vol. 28, pp. 1142-1153, 2007.

26. T. Roy and D. Chakraborty, Delamination in FRP Laminates with Holes Under Transverse Impact, *Materials & Design*, vol. 29, pp. 124-132, 2008.

27. S.K. Panigrahi and B. Pradhan, Onset and Growth of Adhesion Failure and Delamination Induced Damage in Double Lap Joint of Laminated FRP Composites. *Composite Structures*, vol. 85, pp. 326-336, 2008.

28. A.N. Palazotto,E.J. Herup and L.N.B. Gummadi, Finite Element Analysis of Low-Velocity Impact on Composite Sandwich Plates, *Compos. Structures*; vol.49, pp. 209–27, 2000.

29. L. Kärger, J. Baaran and J. Teßmer, Rapid Simulation of Impacts on Composite Sandwich Panels Inducing Barely Visible Damage, *Compos. Structures*, vol. 79, pp. 527–34, 2007.

30. A. Diaz Diaz, J.J. Caron and A. Ehrlacher, Analytical Determination of the Modes I, II and III Energy Release Rates in a Delaminated Laminate and Validation of a Delamination Criterion, *Composite Structures*, vol. 78, pp. 424-432, 2007.

31. U. Icardi and L. Ferrero, Impact Analysis of Sandwich Composites Based on a Refined Plate Element with Strain Energy Updating, *Composite Structures*, vol. 89, pp. 35-51, 2009.

32. A.K. Noor and M. Malik, An Assessment of Modelling Approaches for Thermo-Mechanical Stress Analysis of Laminated Composite Panels, *Computat. Mechanics*, vol. 25, pp.43–58, 2000.

33. Y. Zhang and C. Yang, Recent Developments in Finite Element Analysis for Laminated Composite Plates, *Composite Structures*, vol. 88, pp. 147-157, 2009.

34. J.N. Reddy and R.A. Arciniega, Shear Deformation Plate and Shell Theories: from Syavsky to Present, *Mech Advanced Mater & Struct*, vol. 11, pp.535-582, 2004.

35. Y.M. Ghugal and R.P. Shimpi, A Review of Refined Shear Deformation Theories of Isotropic and Anisotropic Laminated Plates, *J Reinforced Plastics & Composites*, 2001, vol. 20, pp.255-272.

36. J.N. Reddy, *Mechanics of LaminatedCcomposite Plates - Theory and Analysis*, 2nd Edition, CRC Press, Boca Raton, FL., 2003.

37. N. Noda and R.B. Hetnarski, Y. Tanigawa, *Thermal Stresses*, 2nd Edition, Taylor & Francis, New York, 2003.

38. R.B. Hetnarski and R. Eslami, *Thermal Stresses-Advanced Theory and Applications*, Springer, 2009.

39. S. Hashemi, A.K. Kinloch and J.G. Williams, The Effects of Geometry, Rate and Temperature on the Mode I, Mode II and Mixed-mode I/II Interlaminar Fracture of Carbon-Fiber Polyether-Ether Ketone Composites, *J. Composite Materials*, vol. 24, pp:918-956, 1990.

40. B. Fiedler, M. Hojo and S. Occhiai, The influence of the Thermal Residual Stresses on the Transverse Strength of CFRP using FEM, *Composites: Part A*, vol. 33, pp. 1323-1326, 2002.

41. O. Sayman, Analysis of Multi-Layered Composite Cylinders Under Hygrothermal Loading, *Composites: Part A*, vol. 36, pp. 923-933, 2005.

42. J.A. Nairm, Energy Release Rate Analysis for Adhesive and Laminate Double Cantilever Beam Specimens Emphasizing the Effect of Residual Stresses. *Int. J. Adhes. & Adhesives*, vol. 20, pp: 59-70, 2000.

43. M.M. Aghdam and A. Khojeh, More on the Effects of Thermal Residual and Hydrostatic Stresses on Yielding Behaviour of Unidirectional Composites, *Composite Structures*, vol. 62, pp. 285-290, 2003.

44. X. Shu, Thermoelastic Delamination of Composite Laminates with Weak Interfaces. *Composite Structures*, vol. 84, pp. 310-318, 2008.

45. S.K. Panda and B. Pradhan, Thermoelastic Analysis of the Asymmetries of Interfacial Embedded Delamination Characteristics in Laminated FRP Composites. *Composites Part A*, vol. 38, pp. 337-347, 2007.

46. B. Pradhan and S.K. Panda, The Influence of Ply Sequence and Thermoelastic Stress Fields on Asymmetric Delamination Crack Growth Behavior of Embedded Elliptical Delaminations in Laminated FRP Composites, *Composites Sci. & Technology*, vol. 66, pp. 417-426, 2006.

47. P.R. Babu and B. Pradhan, Thermoelastic Effects on Mixed-Mode Delamination Growth Emanating from Circulkar Holes in Laminated FRP Composites, *Composite Structures*, vol. 82, pp. 50-60, 2008.

48. A. Hattiangadi and T. Siegmund, A Thermomechanical Cohesive Zone Model for Bridged Delamination Cracks, *J Mech Physics Solids*, vol. 52, pp. 533-566, 2004.

49. U. Icardi, Multilayered Plate Model with "Adaptive" Representation of Displacement and Temperature Across the Thickmess and Fixed d.o.f., *J Thermal Stresses*, vol. 34, pp. 958-984, 2011.

50. U. Icardi and G. Zardo, C° Plate Element for Delamination Damage Analysis, Based on a Zig-Zag Model and Strain Energy Updating, *Int. J. Impact Engineering*, vol. 31, pp. 579-606, 2005.

51. M. Cho, K.O. Kim andM.H. Kim, Efficient Higher-Order Shell Theory for Laminated Composites, *Composite Structures*, vol. 34, pp. 197-212, 1996.

52. M. Di Sciuva, Bending, Vibration and Buckling of Simply-Supported Thick Multilayered Orthotropic Plates: an Evaluation of a New Displacement Model, *Jnl. Sound & Vibration*, vol. 105, pp. 425–442, 1986.

53. X. Li and D. Liu, Generalized Laminate Theories Based on Double Superposition Hypothesis, *Int. J. Numer. Meth. Engineering*, vol. 40, pp. 1197–212, 1997.

54. V.R. Aitharaju, R.C. Averill, C^0 Zig-Zag Kinematic Displacement Models for the Analysis of Laminated Composites, *Mech. of Comp. Mater. & Struct*ures, vol. 6, pp. 31-56, 1999.

55. H. Murakami, Laminated Composite Plate with Improved In-Plane Responses, *J. Appl. Mechanics*, vol. 53, pp.661-666, 1986.

56. S. Kapuria, P.C.Dumir and A. Ahmed, An Efficient Higher Order Zigag Theory for Composite and Sandwich Beams Subjected to Thermal Loading, *Int. J. Solids & Structures*, vol. 40, pp. 6613–6631, 2003.

57. J. Oh and M. Cho, A Finite Element Based on Cubic Zig-zag Plate Theory for the Prediction of Thermo-Electric-Mechanical behaviors, *Int. J.Solids & Structures*, vol. 41, pp.1357–1375, 2004.

58. U. Icardi and L. Ferrero, Multilayered Shell Model with Variable Representation of Displacements Across the Thickness, *Composites: Part B*, vol. 428, pp.18-26, 2011.

59. U. Icardi and A. Atzori, Simple, Efficient Mixed Solid Element for Accurate Analysis of Local Effects in Laminated and Sandwich Composites, *Advances in Eng Software*, vol. 32, pp. 843-859, 2004.

60. L. Iannucci, Dynamic Delamination Modelling Using Interface Elements, *Computers & Structures*, vol. 84, pp. 1029-1048, 2006.

61. M. Nishikawa, T. Okabe and N. Takeda, Numerical Simulation of Interlaminar Damage Propagation in CFRP Cross-Ply Laminates under Transverse Loading, *Int. J of Solids & Struct*, vol. 44, pp. 3101-3113, 2007.